https://doi.org/10.5194/egusphere-2026-2809
Preprint. Discussion started: 6 July 2026

Permafrost thaw reshapes methane cycling across an interior Alaska peatland

Hailey Webb[1,2], Clifton P. Bueno de Mesquita[1,3], Mario E. Muscarella[4], Catherine M. Dieleman[5], Eugénie S. Euskirchen[4], Evan S. Kane[6], Jason K. Keller[7,8], Steven K. Schmidt[1], Amanda Stromecki[4], Merritt R. Turetsky[1,2]

[1]Department of Ecology and Evolutionary Biology, University of Colorado Boulder, Boulder, CO, USA
[2]Renewable and Sustainable Energy Institute, University of Colorado Boulder, Boulder, CO, USA
[3]Cooperative Institute for Research in Environmental Sciences, University of Colorado Boulder, Boulder, CO, USA
[4]Institute of Arctic Biology, University of Alaska Fairbanks, Fairbanks, AK, USA
[5]School of Environmental Sciences, University of Guelph, Ontario, Canada
[6]Michigan Technological University, College of Forest Resources and Environmental Science, Houghton, MI, USA
[7]Kravis Department of Integrated Sciences, Claremont McKenna College, Claremont, CA, USA
[8]Schmid College of Science and Technology, Chapman University, Orange, CA, USA

Correspondence to: Hailey Webb (hailey.webb@colorado.edu)

Abstract. Permafrost thaw is expected to increase methane (CH_4) emissions from northern peatlands, but it remains uncertain how thaw affects the microbial pathways driving CH_4 production and oxidation. We measured CH_4 and carbon dioxide (CO_2) fluxes during July 2022 using static chambers and combined these measurements with δ^{13}C-CH_4 measurements, 16S rRNA and mcrA gene sequencing, as well as environmental data across a fine-scale thaw gradient in an interior Alaska peatland. Mean CH_4 fluxes increased from near neutral (-0.1 ± 0.02 μmol m^{-2} s^{-1}) in stable thaw stages to 40.2 ± 12.0 μmol m^{-2} s^{-1} in advanced thaw stages, while CO_2 fluxes did not change. Thaw progression was associated with higher water tables and deeper seasonal thaw depths with an increase in methanogen relative abundance and shift in methanogen community composition. Hydrogenotrophic taxa increased in relative abundance with advanced thaw along the gradient, particularly *Methanoregula*, which explained 36% of the variability in CH_4 fluxes. Despite this shift, emitted δ^{13}C-CH_4 values fell within ranges commonly attributed to acetoclastic methanogenesis. Rayleigh fractionation modeling suggests that ~ 40% of CH_4 produced at depth was oxidized before reaching the atmosphere, enriching residual CH_4 in ^{13}C and altering the isotopic signature of emitted fluxes. These results highlight the need to integrate fluxes, isotopes, and microbial community data to fully resolve CH_4 cycling processes in thawing permafrost peatlands.

1 Introduction

Permafrost underlies ~15% of the land surface in the northern hemisphere (Obu, 2021) and stores 1,460-1,600 Pg organic carbon, comprising nearly half of global belowground soil carbon stocks (Hugelius et al., 2014; Schuur et al., 2022). As subarctic and Arctic temperatures rise at two to four times the global average (Rantanen et al., 2022; Salehnia et al., 2025), widespread permafrost thaw is making previously frozen carbon available for microbial decomposition (Chen et al., 2021). This decomposition releases carbon as carbon dioxide (CO_2) under both oxic and anoxic conditions, and as methane (CH_4)

https://doi.org/10.5194/egusphere-2026-2809
Preprint. Discussion started: 6 July 2026

primarily under anoxic conditions. Although CO_2 is more abundant in the atmosphere, CH_4 has a global warming potential approximately 30 times greater than CO_2 over a 100-year timescale (Bäck et al., 2024). Therefore, even small increases in CH_4 emissions from thawing permafrost ecosystems have the potential to substantially amplify climate warming. The total magnitude of CH_4 emissions from Arctic and subarctic regions remains one of the largest uncertainties in projections of the permafrost-climate feedback (Burke et al., 2012; Knoblauch et al., 2018).

Northern peatlands are particularly important within the permafrost carbon pool, storing ~450-500 Pg carbon (Harris et al., 2022). Northern peatlands typically function as long-term CO_2 sinks due to high primary productivity and low decomposition (Helbig et al., 2022; Qiu et al., 2020). However, ground ice melt from thawing permafrost often causes surface subsidence and rising water tables, transforming peat plateaus into water-saturated and oxygen-poor collapse-scar bogs (Jorgenson et al., 2022; Swindles et al., 2015). These hypoxic to anoxic conditions promote methane production, potentially shifting these long-term carbon sinks into substantial CH_4 sources.

Methane is produced by archaea via three main pathways: acetoclastic, hydrogenotrophic, and methyl-based methanogenesis, all of which have distinct isotopic CH_4 signatures (Whiticar, 1999; Whiticar et al., 1986). Acetoclastic methanogenesis converts acetate into CO_2 and CH_4 and typically dominates in environments with abundant labile organic substrates (Chasar et al., 2000). Hydrogenotrophic methanogenesis often occurs in nutrient-poor, acidic peatlands and is the process by which CO_2 is reduced by H_2, producing CH_4 (Horn et al., 2003). Methyl-based methanogenesis (including the methyl-dismutation and methyl-reducing pathways) transforms methylated compounds such as methanol and methylamines into CH_4 and may be common in organic-rich peat systems where these types of substrates accumulate (Bueno de Mesquita et al., 2023; Zalman et al., 2018). However, the isotopic signatures of CH_4 may also be modified by CH_4 oxidation along the soil profile. Methanotrophs preferentially consume $^{12}CH_4$, enriching residual CH_4 in ^{13}C prior to atmospheric release (Templeton et al., 2006; Wang et al., 2016). By altering environmental conditions such as water table and substrate availability, permafrost thaw is expected to restructure methanogenic communities and alter CH_4 production pathways, shifting the isotopic composition of emitted CH_4 (McCalley et al., 2014). Although permafrost thaw has been associated with shifts in microbial communities, δ^{13}C-CH_4 isotopic signatures, and CH_4 emissions (Holm et al., 2020; Liebner et al., 2015; McCalley et al., 2014; Waldrop et al., 2021), translating these shifts into predictions of CH_4 production pathways and emissions remains challenging. Some studies in interior Alaska have measured increased methanogenesis activity following permafrost thaw (Kuhn et al., 2024; Waldrop et al., 2021), but the extent to which methanogen communities shift along a thaw gradient and the associated shifts in ecosystem CH_4 emissions and δ^{13}C-CH_4 signatures are not well understood.

To address this knowledge gap, we measured CO_2 and CH_4 fluxes, δ^{13}C-CH_4 signatures from porewater and chamber gas, and key environmental variables including water table depth, seasonal thaw depth, soil temperature, and soil moisture across 32 sampling collars spanning stable permafrost to permafrost undergoing early, intermediate, and advanced thaw. Soil cores were

https://doi.org/10.5194/egusphere-2026-2809
Preprint. Discussion started: 6 July 2026

used to characterize total microbial community composition (16S rRNA gene) and methanogenic communities (mcrA gene) along the soil profile. By linking these variables from the field, this study provides a mechanistic framework for understanding how methanogen restructuring drives CH_4 production and pathway shifts across an Interior Alaskan peatland thaw gradient.

2 Methods

2.1 Site Description

The study site, named Beta, is a permafrost peatland with a collapse-scar bog located about 30 km southwest of Fairbanks near the Tanana River in interior Alaska (Figure 1) (64.6962470, -148.3213389). It is part of the Alaska Peatland Experiment (APEX) within the broader Bonanza Creek Long Term Ecological Research (LTER) Network (Chapin et al., 2006). The area is characterized by a subarctic continental climate with long, cold winters and short, warm summers. Based on the National Oceanic and Atmospheric Administration (NOAA) 30-year climate normals (1994-2024), the region has a mean annual temperature of approximately -2 °C and receives an average of 30.4 cm of precipitation annually (NOAA National Centers for Environmental information).

https://doi.org/10.5194/egusphere-2026-2809
Preprint. Discussion started: 6 July 2026

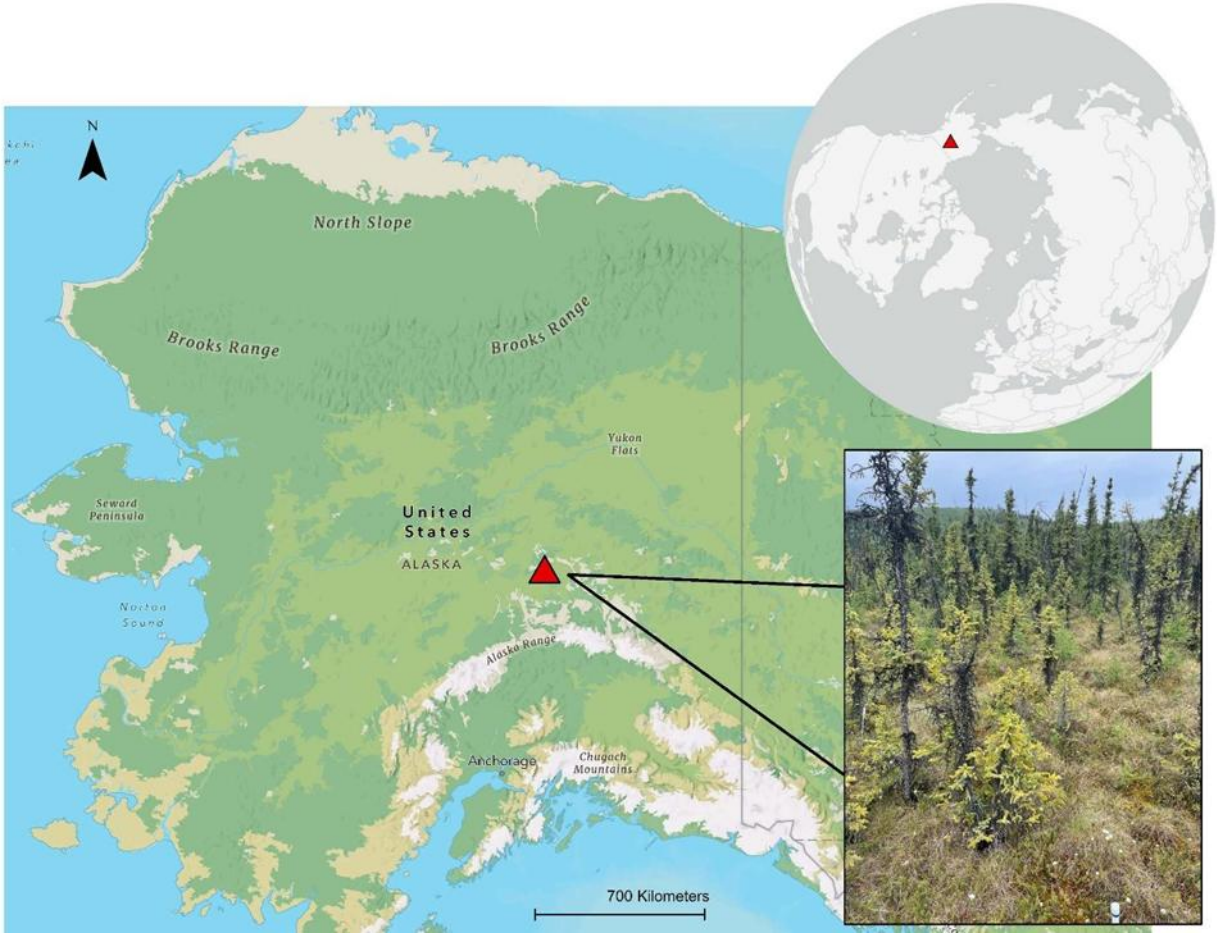

Figure 1. Map of Alaska showing the study site located near Fairbanks, Alaska, USA.

Beta consists of a permafrost plateau containing stable- and early-stage thawing permafrost and an active thaw margin with intermediate- to advanced- stage permafrost thaw (Figure S1). The permafrost plateau is characterized by black spruce (*Picea mariana*), American larch (*Larix laricina*), shrubs (including *Betula glandulosa* Michx., *Vaccinium oxycoccus*, *Vaccinium vitis-idaea*, *Rubus chamaemorus*), and *Sphagnum* spp. mosses. The active thaw margin is at the edge of a moving thaw front, dominated by subsiding black spruce trees, sedges (*Carex aquatilis*), tussock cottongrass (*Eriophorum vaginatum*) and *Sphagnum* spp. mosses. There are 32 established research plots across the thaw gradient (20 in the permafrost plateau; 12 in the active thaw margin), supporting over a decade of long-term monitoring of soil properties, vegetation dynamics, and CO_2 and CH_4 fluxes. Research plots are grouped into one of four permafrost thaw stages: stable, early, intermediate, or advanced, based on active layer thickness measurements in September spanning several years (Cox et al., 2025; Figure S2).

https://doi.org/10.5194/egusphere-2026-2809
Preprint. Discussion started: 6 July 2026

2.2 Environmental data and soil core collection

Environmental variables were measured at each plot during July 2022. Water table depth and soil temperature were measured seven times throughout the month via permanently installed PVC wells adjacent to each soil collar and a handheld thermometer, respectively . Water table depth was calculated by subtracting the distance between the soil surface and the top of the well from the distance between the top of the well to the water surface inside the PVC. Over time, some PVC wells were inundated or covered by vegetation, resulting in missing water table measurements for a subset of collars (n = 5). Seasonal thaw depth was measured weekly (four measurements total) using a 120 cm metal frost probe to resistance. Depths exceeding the probe length were recorded as the maximum measurable depth. Soil moisture data was quantified using a Dynamax HH2 soil moisture sensor (Dynamax, Houston, USA); however, due to instrument malfunction values were unavailable for the 2022 field season. Instead, July 2021 soil moisture measurements (two sampling dates) were used to characterize relative moisture conditions among plots. While absolute soil moisture conditions likely differed in 2022 due to unusually dry conditions relative to the preceding 12 summers, relative differences among plots are expected to be broadly consistent. Therefore, results should be interpreted with caution since soil moisture values reflect conditions from the previous year.

A soil core of the seasonally thawed (unfrozen) layer was collected at each plot using a 90-cm long, 4.5-cm diameter, handcrafted stainless steel corer. The corer was disinfected between samples by pulling an ethanol-soaked paper towel through the interior and wiping the exterior. Fresh nitrile gloves were worn for each core and for each core section. Cores were sectioned in the field into three depth intervals relative to the depth of the seasonally thawed layer: shallow (0-15 cm), intermediate (15-30 cm), and deep (30-45 cm) using a stainless steel bread knife sterilized with ethanol between cuts to minimize cross-contamination. In plots where the seasonal thaw depth was shallower than 45 cm, cores were sectioned only to the depth of ice. All samples (n = 101) were immediately transported to the University of Alaska Fairbanks and stored at -80 °C until molecular analysis.

2.3 CO_2 and CH_4 fluxes

Soil flux chambers were constructed of 0.6-cm thick polycarbonate (Lexan) with an internal chamber volume of 0.23 m^3 and ground area of 0.36 m^2. Chambers were fitted with two internal CPU fans to ensure proper gas mixing, two sample ports, and were designed to seal via foam into previously established soil collars. Gas concentrations used in this study were taken from three sampling campaigns in July 2022. Carbon dioxide and CH_4 concentrations were measured every 1 – 3 seconds and averaged over a 5 second interval using a GasScouter™ G4301 Mobile Gas Concentration Analyzer (Picarro, Santa Clara, USA). Each soil collar was sampled for three minutes with a transparent chamber to capture CO_2 dynamics under natural light conditions, after which the chamber was vented to equalize with ambient environmental conditions, shrouded to fully exclude natural light, and then sealed for additional three minutes to quantify shifts in CH_4 — following the methods outlined in Cox

https://doi.org/10.5194/egusphere-2026-2809
Preprint. Discussion started: 6 July 2026

et al. (2025). The first and last 5 seconds of gas flux measurements were removed to minimize error due to chamber placement, and fluxes were calculated from the raw gas concentration data using linear regression and the ideal gas law (Equation 1):

$$Flux = \frac{\left(\frac{dC}{dt}\right) * P * V}{R * T * A} \quad (1)$$

$\frac{dC}{dt}$ = slope of the concentration over time (ppm sec^{-1})

P = atmospheric pressure (101,325 Pa)

V = soil chamber volume (0.23 m^3)

R = universal gas constant (8.314 m^3 Pa mol^{-1} K^{-1})

T = chamber air temperature (K)

A = ground surface area (0.36 m^2)

Carbon dioxide fluxes are reported in µmol m^{-2} s^{-1} while CH_4 fluxes are reported in µmol m^{-2} min^{-1}. Light measurements were used for CO_2 flux analyses to represent net ecosystem exchange (NEE) while dark measurements were used for CH_4 flux analyses to control for influence from light-dependent CH_4 processes (King, 1990). Two extreme CH_4 uptake values were investigated and found to originate from chambers with elevated CH_4 concentrations (~14 ppm) at the start of sampling, likely caused by ebullition events from placing the chambers on the collar. Because these conditions do not represent ambient starting concentrations and were not consistent with starting concentrations of other chambers, these measurements were excluded from further analysis. Initial CO_2 concentrations during these measurements were within ambient ranges, indicating that the issue was specific to CH_4.

2.4 Chamber and porewater δ^{13}C- CH_4 sampling

Gas samples for δ^{13}C-CH_4 analyses were collected during two sampling campaigns in July 2022 using two complementary approaches. The first approach involved collecting chamber headspace gas using evacuated Exetainers (Labco, Lampeter, UK). Prior to field sampling, 12-mL Exetainers were evacuated for 2 minutes each using a GE commercial A-C motor vacuum pump. In the field, a soil flux chamber (section 2.3) was placed on a soil collar for 30 minutes. At the end of the incubation period, chamber air was pulled through a sampling port using a 20-mL plastic syringe fitted with a stopcock. A hypodermic needle was then attached to the syringe, and the full 20-mL gas sample was injected into a pre-evacuated 12-mL Exetainer. Two Exetainers were filled per sampling period to provide replicate measurements. However, only two samples from stable plots had high enough CH_4 concentrations for analytical detection.

The second approach involved extracting dissolved gases from porewater following similar methods to Corbett et al. (2013). In the laboratory, 60-mL glass serum bottles were cleaned, dried, sealed with rubber septa, and crimped with aluminum caps.

https://doi.org/10.5194/egusphere-2026-2809
Preprint. Discussion started: 6 July 2026

Bottles were evacuated for 5 minutes using the same vacuum pump, and additional Exetainers were prepared as described above. At plots with sufficient porewater availability (n = 26), porewater was collected from 33 cm and 100 cm depths using 60-mL plastic syringes fitted with disposable hypodermic needles and a stainless steel sipper tube (100 cm length) with a 2 cm slotted intake region wrapped in 35 µm nylon mesh. A total of 30 mL of porewater was injected into each pre-evacuated serum bottle, which was immediately stored in a cooler with ice packs for transport. Porewater samples could not be collected at stable collars due to insufficient water in the soil profile.

In the laboratory, the headspace of each serum bottle was flushed with ultra-high purity nitrogen for 1 minute. Bottles were then vigorously shaken for 2 minutes to free dissolved gases from the porewater. Immediately after shaking, 15 mL of headspace gas was withdrawn using a 20 mL syringe with a hypodermic needle and transferred into the evacuated 12-mL Exetainers. The Exetainers from both sampling approaches were sent to Chapman University for analysis on a Picarro G2201-i isotopic analyzer equipped with a small sample isotope module (Picarro, Santa Clara, USA). A 2-mL subsample from each Exetainer was injected for analysis of CO_2 and CH_4 concentrations and isotopes. Standard curves for both concentrations and isotopes were generated using 2-mL subsamples from Exetainers containing standards.

Chamber and porewater δ^{13}C-CH_4 data were post-processed to account for high variability associated with low CH_4 concentrations, which can lead to increased analytical uncertainty on the Picarro analyzer. The instrument reports a standard deviation for each isotopic measurement; therefore, measurements with standard deviations greater than 10 were considered unreliable and excluded from analyses. These high-uncertainty values were most associated with samples containing CH_4 concentrations below 5 ppm. For plots with multiple measurements across sampling approaches and duplicates, δ^{13}C- CH_4 values were averaged prior to statistical analyses.

Methanogenic pathways were inferred from δ^{13}C-CH_4 values using established isotopic thresholds from the literature (Hornibrook et al., 2000; Whiticar, 1999; Whiticar et al., 1986). Hydrogenotrophic methanogenesis, which produces CH_4 from CO_2 and H_2, is associated with more negative δ^{13}C-CH_4 values and is typically in the range of -110‰ to -60‰. Acetoclastic methanogenesis converts acetate to CH_4 and generally results in δ^{13}C-CH_4 values between -65‰ to -50‰. Methylotrophic methanogenesis, which produces CH_4 from methylated substrates such as methanol and methylamines, typically yields δ^{13}C-CH_4 values that overlap those of acetoclastic and hydrogenotrophic pathways, commonly ranging from approximately -90‰ to -50‰ depending on substrate isotopic composition and fractionation factors (Penger et al., 2012; Whiticar, 1999). Interpretation δ^{13}C-CH_4 values also considers the effects of CH_4 oxidation which can cause enrichment (less negative values). These values were cross-referenced with microbial sequencing data to strengthen the interpretation of dominant methanogenic pathways.

Apparent carbon isotope fractionation between CO_2 and CH_4 (α_C) was calculated using the following equation:

https://doi.org/10.5194/egusphere-2026-2809
Preprint. Discussion started: 6 July 2026

$$\alpha_C = \frac{\delta^{13}CO_2 + 1000}{\delta^{13}CH_4 + 1000} \quad (2)$$

Where δ values are expressed in ‰ relative to VPDB. Fractionation factors were calculated separately for each depth (shallow, deep) and chamber flux samples (also referred to as surface depth). Apparent fractionation values were interpreted using the following thresholds: α_C < 1.055 (acetoclastic dominant), 1.055–1.065 (mixed), and > 1.065 (hydrogenotrophic dominant). Methylotrophic methanogenesis is not associated with a distinct apparent fractionation range and often overlaps with both acetoclastic and hydrogenotrophic pathways (Whiticar 1999).

To estimate CH_4 oxidation during upward transport in the soil profile, we used a Rayleigh fractionation model to calculate the fraction of CH_4 remaining (f) based on isotopic enrichment between deep porewater and chamber CH_4 (Clark and Fritz, 1998). The fraction remaining was calculated as:

$$f = exp\left(\frac{\delta - \delta_0}{\varepsilon}\right) \quad (3)$$

f = fraction of remaining CH_4
δ_0 = initial CH_4 isotope composition (deep porewater)
δ = enriched surface CH_4 (chamber flux)
ε = carbon isotope enrichment factor associated with CH_4 oxidation (-15‰)

The percent of CH_4 that was oxidized was then calculated as $(1 - f) * 100$.
An isotopic enrichment factor of ε = -15‰ was used as a conservative, mid-range value reported for CH_4 oxidation (Templeton et al., 2006; Wang et al., 2016; Whiticar, 1999). The Rayleigh model assumes that CH_4 is oxidized in a closed system. However, soils represent an open system where CH_4 is continuously produced and diffused. Because diffusion can cause isotopic enrichment, our calculated oxidation percentages represent apparent rather than absolute oxidation rates.

2.5 Microbial sequencing

2.5.1 DNA Extraction

Soils were stored at -80 ºC until molecular analysis. Soil was manually homogenized with a sterile spatula in a petri dish, and 0.25 g of homogenized soil (wet weight) was used for each DNA extraction. DNA was extracted from all samples (n = 101) using the ZymoBIOMICS DNA Miniprep Kit according to the manufacturer's protocol (Zymo Research, Irvine, CA).

https://doi.org/10.5194/egusphere-2026-2809
Preprint. Discussion started: 6 July 2026

Following extraction, DNA was quantified using a Qubit with the HS dsDNA Quantification Kit (Invitrogen, Waltham, USA), and a subset of samples was tested for PCR inhibitors using a 16S rRNA PCR assay (see Supplemental).

2.5.2 Microbial community composition

To determine the composition of bacteria and archaea in each sample, we used the 16S rRNA gene as a taxonomic marker. 16S rRNA genes were amplified in triplicate 25 µL PCR reactions using barcoded forward primers 515F (GTGYCAGCMGCCGCGGTAA) and 926R (GGACTACNVGGGTWTCTAAT) (Apprill et al., 2015; Parada et al., 2016). Briefly, each reaction contained 12.5 µL Platinum™ Taq Master Mix, 0.5 µL of each primer, 2 µL of DNA template (final concentration ~10 ng), and 9.5 µL molecular-grade water. Negative controls contained molecular-grade water in place of template DNA, and positive controls contained *Escherichia coli* (*E.coli)* genomic DNA. Thermal cycling consisted of 95°C for 3 minutes, followed by 30 cycles of 95°C for 45 seconds, 55°C for 30 seconds, and 72°C for 90 seconds, with a final extension at 72°C for 10 minutes and a 4°C hold. Amplicons (V4-V5 region) were verified by agarose gel electrophoresis. Triplicate samples were pooled and cleaned using Sera-Mag Beads (Cytiva, Marlborough, USA) at a 1:1 ratio. Cleaned products were quantified using the Quant-IT fluorometric quantification kit (Invitrogen). Final products were pooled into a library at equal molar ratios (20 ng per sample). The library was quantified using a Qubit, run on an Agilent TapeStation to confirm size (D1000 reagents; Agilent), and tested for Illumina adapters using a P5-P7 PCR assay (see Supplemental). The final library was submitted for sequencing at the University of Alaska Fairbanks Genomics Core Lab and was sequenced on an Illumina MiSeq using 300 x 300 V3 chemistry.

Sequences were processed with the DADA2 pipeline (Callahan et al. (2016) to quality filter reads, infer amplicon sequence variants (ASVs), and assign taxonomy using the SILVA 138.2 database (Chuvochina et al., 2026). Chloroplast and mitochondrial DNA were removed from the dataset, as were any sequences not assigned to archaeal or bacterial domains. To assign functional guilds from the 16S rRNA gene sequencing data, including methanogens and methanotrophs, we used a custom guild-calling script developed by Hartman et al. (2024) based on known taxonomy-function relationships.

2.5.3 mcrA primer testing and positive control construction

To validate mcrA amplification, we initially tested the ML_mcrA_F (GGTGGTGTMGGATTCACACARTAYGCWACAGC) and ML_mcrA_R (TTCATTGCRTAGTTWGGRTAGTT) primers on 12 randomly selected DNA samples. Successful amplicons were cloned into *E.coli*, and five plasmid clones were sequenced using Sanger Sequencing (GeneWiz, South Plainfield, USA) to confirm the identity of the mcrA insert. These plasmid constructs were purified using a PureLink Quick Plasmid MiniPrep Kit (Invitrogen), stored at -20°C, and used as positive controls for subsequent PCR reactions.

https://doi.org/10.5194/egusphere-2026-2809
Preprint. Discussion started: 6 July 2026

2.5.4 mcrA gene amplification and sequencing

To determine the diversity and variability of mcrA genes in each sample, we amplified a ~475 base pair fragment of the mcrA gene using custom ML_mcrA_F and ML_mcrA_R primers that contained iTru adapters (Glenn et al., 2019) (see Supplemental). Each sample was amplified in triplicate using 25 µL PCR reactions containing 12.5 µL Platinum™ Taq Master Mix, 0.5 µL of each primer (10mM), 2 µL of DNA template, and 9.5 µL molecular-grade water. Positive controls contained 2 µL plasmid standard (see above) and negative controls contained 2 µL molecular-grade water. Thermal cycling consisted of 95°C for 5 minutes, followed by 30 cycles of 95°C for 45 seconds, 55°C for 45 seconds, and 72°C for 90 seconds, with a final extension at 72°C for 10 minutes and a 4°C hold. Samples that failed to amplify on the first attempt were re-run using 5 µL DNA and 6.5 µL water to improve amplicon efficiency. PCR products were confirmed by agarose gels prior to downstream analyses. A secondary limited-cycle PCR was performed to add barcoded iTru adapters (see Supplemental). Triplicate samples were pooled and cleaned using Sera-Mag Beads at a 1:1 ratio. Cleaned products were quantified using the Quant-IT flurometric quantification kit (Invitrogen) and final products were pooled into a library at equal molar ratios (20 ng per sample). The library was quantified using a Qubit, run on a TapeStation (D1000 reagents; Agilent) to confirm size. The final library was submitted for sequencing at the University of Alaska Genomic Core Lab and was sequenced on an Illumina MiSeq using 300 x 300 V3 chemistry.

Sequences were processed using the DADA2 pipeline. Adapters were removed using cutadapt (Martin 2011) and individual sequences were trimmed based on sequence quality using the denoise-single function following visual inspection. We used the forward reads only because there was not sufficient overlap with the reverse reads after quality trimming. Sequences were binned into ASVs, and representative sequences were generated using the DADA2 export function. Taxonomic identities of mcrA gene sequences were determined using the Genome Taxonomy Database (Parks et al., 2026; GTDB). Representative sequences were compared to the GTDB r226 reference database using BLAST+ v 2.17.0 (Camacho et al., 2009). Taxonomy was assigned based on the top-scoring BLAST hit if the alignment had ≥ 90% amino acid identity and an alignment length of ≥ 60 amino acids. Hits not meeting these criteria were excluded from taxonomic assignment. Taxonomy was assigned at the lowest supported rank, including GTDB species-level identifiers which may represent placeholder names for uncultured taxa.

2.6 Statistical analyses

All figures were made with the ggplot2 R package (Wickham, 2016) and all statistical analyses were performed with R 4.5.1 (R Core Team, 2025). Environmental variables (water table depth, seasonal thaw depth, soil temperature, and volumetric soil moisture) were analyzed using linear mixed-effects models, implemented with the lmerTest package (Kuznetsova et al., 2013). Site and thaw stage were included as fixed effects and plot ID as a random effect to account for repeat measures.

https://doi.org/10.5194/egusphere-2026-2809
Preprint. Discussion started: 6 July 2026

Differences in CO_2 and CH_4 flux between thaw stages were assessed using linear-mixed effects models with thaw stage as a fixed effect and plot ID as a random effect to account for repeated measurements. Because raw CH_4 fluxes were heavily right-skewed, the data were transformed using a signed square root which preserves the original sign of each flux while taking the square root of its absolute value. This transformation addresses deviations from normality and maintains the direction of the flux (i.e., uptake vs. emissions) (Hansen et al., 2025; Klaus et al., 2024).

To evaluate the effects of thaw progression and soil depth on δ^{13}C-CH_4, we fit a linear mixed-effects model with repeated measurements including thaw stage (early, intermediate, advanced), depth (surface, shallow, deep), and their interaction. Stable thaw stages were excluded from mixed-effects model analyses due to insufficient porewater availability, which prevented comparisons along the soil depth profile.

For all microbial analyses, all samples were rarefied to a uniform sequencing depth to minimize biases associated with uneven sequencing effort (16S rRNA = 3,635; mcrA = 4,498) while still capturing the diversity of the communities (Schloss, 2024). Samples with reads fewer than the rarefaction cutoff were removed, leaving 71 samples for the 16S analysis and 80 samples for the mcrA analysis. Community dissimilarity among samples was quantified using Bray-Curtis dissimilarity, and patterns in microbial community composition were visualized using non-metric multidimensional scaling (NMDS), implemented with the mctoolsr R package (Leff, 2022). Ordination quality was assessed using stress values, with stress < 0.2 indicating reliable representation of community structure.

Environmental variables including soil temperature, water table depth, seasonal thaw depth, CH_4 and CO_2 fluxes, and δ^{13}C-CH_4 were fitted to the NMDS ordination using permutation-based vector fitting with the 'envfit' function in the vegan R package (Oksanen et al., 2015). Only vectors with $p \leq 0.05$ were considered significant and kept for interpretation. The best combination of variables associated with community composition was determined with stepwise distance-based redundancy analysis (Legendre and Legendre, 2012), implemented in vegan.

Statistical differences in microbial community composition among thaw stage, core depth, and site were tested using permutational multivariate analysis of variance (PERMANOVA) based on Bray-Curtis dissimilarities and implemented in vegan. To ensure that significant PERMANOVA results reflected differences in community centroids rather than heterogeneous dispersion among groups, multivariate homogeneity of dispersion was evaluated using PERMDISP (Anderson, 2006). No significant differences in dispersion were detected, indicating that observed PERMANOVA results were not biased by unequal within-group variability. Pairwise comparisons were tested using the 'pairwise.perm.manova' function from the RVAideMemoire package (Hervé, 2025).

https://doi.org/10.5194/egusphere-2026-2809
Preprint. Discussion started: 6 July 2026

For 16S rRNA and mcrA sequencing data, taxonomic composition was summarized at multiple taxonomic levels (phylum to species) using relative abundances with mctoolsr. Differences in the relative abundance of dominant taxa among thaw stages were assessed using non-parametric Kruskal-Wallis tests implemented in the mctoolsr package.

3. Results

3.1 Environmental differences along the thaw gradient

Environmental conditions shifted strongly along the permafrost thaw gradient (Figure 2; Supplemental Table S1). Water tables rose and seasonal thaw depths increased with thaw progression ($p < 0.001$). Water tables were ~ 18 – 20 cm higher and seasonal thaw depths ~ 79 cm deeper in advanced thaw stages relative to stable thaw stages. Soil temperature increased by ~ 4 °C in advanced thaw stages ($p < 0.001$), but soil moisture did not vary significantly among thaw stages ($p = 0.32$). However, surface soil moisture exhibited high variability in early and advanced stages.

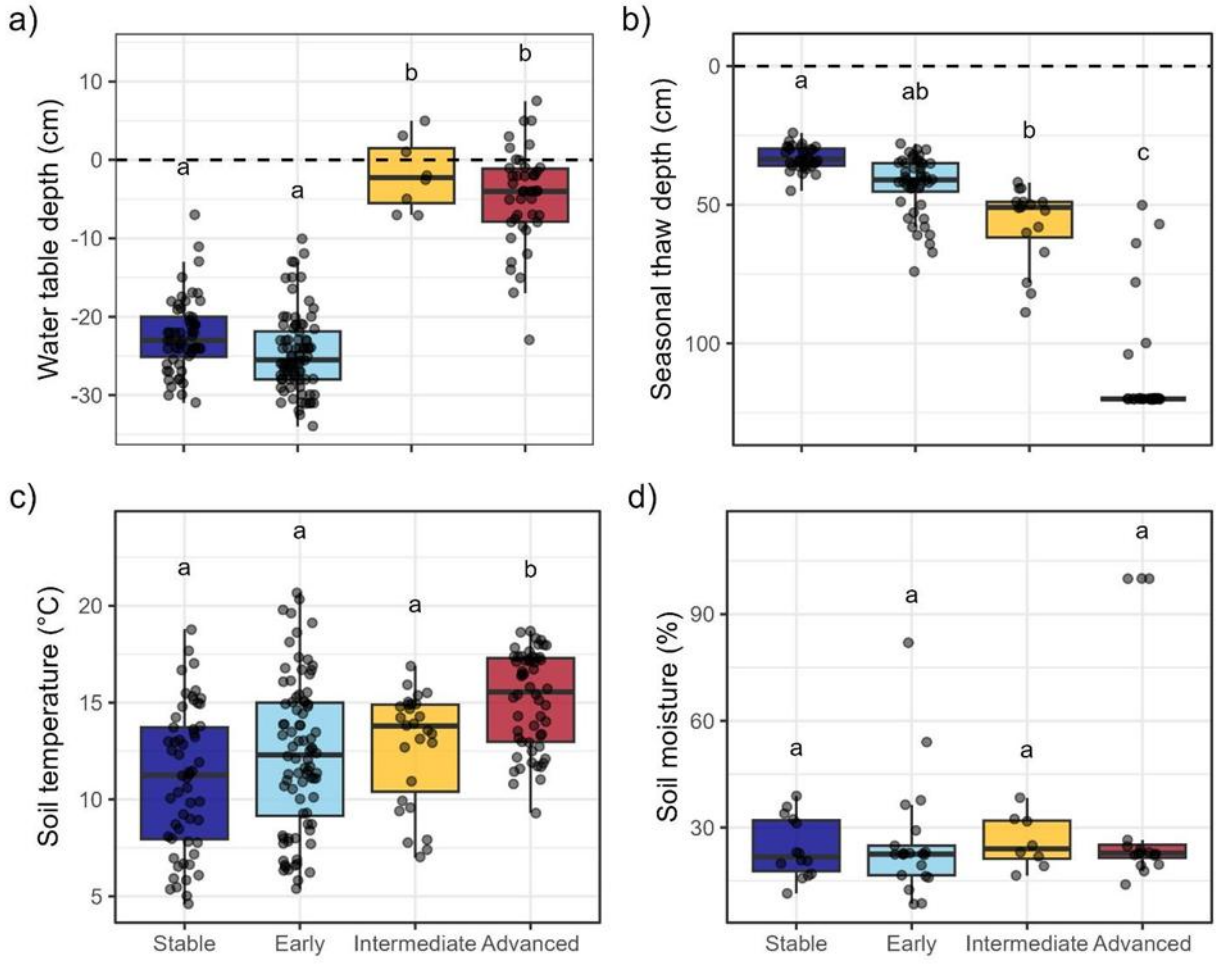

https://doi.org/10.5194/egusphere-2026-2809
Preprint. Discussion started: 6 July 2026

Figure 2. Boxplots showing variation in **a)** water table depth where negative values indicate depth below the soil surface, **b)** seasonal thaw depth, **c)** soil temperature, and **d)** volumetric soil moisture across thaw stages. For panel a, the water table is measured as the distance above or below the ground surface. For panel b, the y-axis is inverted to represent depth below the soil surface so that increasing values indicate deeper seasonal thaw depths. Different letters denote significant differences among thaw stages based on Tukey-Kramer-adjusted pairwise comparisons from linear mixed-effects models. Boxplot center lines indicate the median.

3.2 CO_2 and CH_4 fluxes along the thaw gradient

Carbon dioxide fluxes did not vary across thaw stages ($p = 0.14$). However, the permafrost plateau tended to be a net CO_2 source on average while the active thaw margin was an overall net CO_2 sink (Supplemental Table S2; Figure 3a). The advanced thaw plots tended to be stronger sinks for CO_2 than stable plots, but differences were not significant after multiple comparison adjustment. In contrast, CH_4 emissions varied among thaw stages ($p < 0.001$). Emissions increased consistently from stable to advanced thaw stages, with advanced thaw showing greater CH_4 fluxes than stable and early thaw stages ($p < 0.001$). Only stable plots were net CH_4 sinks while early, intermediate, and advanced thaw stages were all net sources (Table S2; Figure 3b).

https://doi.org/10.5194/egusphere-2026-2809
Preprint. Discussion started: 6 July 2026

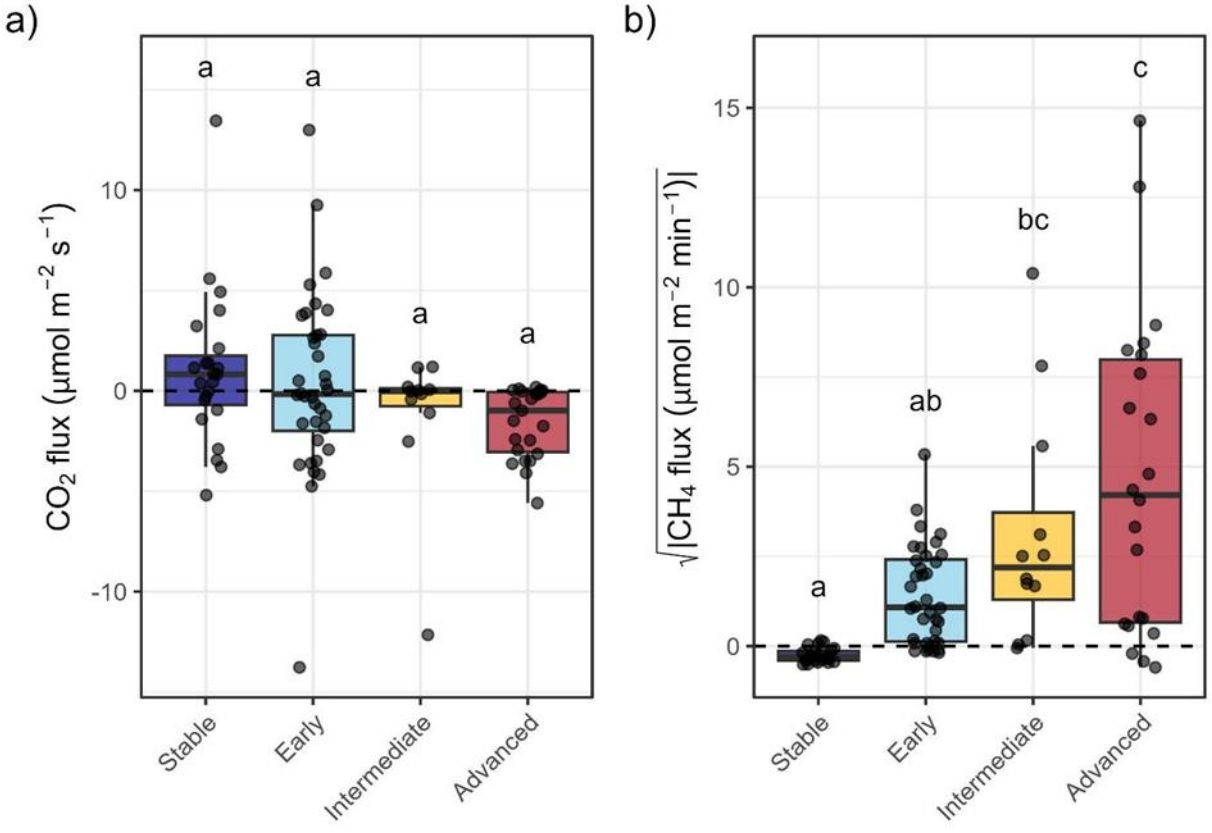

Figure 3. Boxplots of **a)** CO_2 flux (µmol m^{-2} s^{-1}) and **b)** CH_4 flux (µmol m^{-2} min^{-1}) across thaw stages. Negative values represent a sink while positive values reflect a source. Methane flux values were sign-square-root transformed, which preserves the original sign of the flux and takes the square root of its absolute value.

3.3 δ^{13}C-CH_4 isotope shifts with depth and along thaw gradient

δ^{13}C-CH_4 values shifted as thaw progressed and with soil depth ($p < 0.001$; Table 1). The isotopic ranges observed are consistent with values typically associated with acetoclastic methanogenesis. CH_4 from intermediate and advanced thaw was approximately 7-8‰ more ^{13}C-depleted than CH_4 from early thaw, while intermediate and advanced thaw did not differ from one another (Figure 4). δ^{13}C-CH_4 values also varied with depth ($p < 0.001$). Deep porewater CH_4 was approximately 8-9‰ more ^{13}C-depleted (-61.4‰) than CH_4 collected from shallow porewater (-53.5‰) or surface gas (-52.9‰). Methane isotope signatures between surface and shallow measurements did not differ (Figure 4). Additionally, the carbon isotope fractionation factor (α_C) of CH_4 production increased from surface samples to deep samples and along the thaw gradient (Figure 5).

https://doi.org/10.5194/egusphere-2026-2809
Preprint. Discussion started: 6 July 2026

The magnitude of the vertical isotopic gradient was consistent across thaw stages, with no thaw stage x depth interaction (p = 0.46). Although the overall isotopic baseline shifted toward more depleted values with thaw progression, the relative difference between deep and shallow CH_4 remained stable.

Table 1. Results of linear mixed-effects model testing the effects of thaw stage and soil depth on $\delta^{13}C$-CH_4 values across early, intermediate, and advanced thaw stages. Plot ID was included as a random intercept.

Fixed Effect	Numerator DF	Denominator DF	F value	p value
Depth	2	22.8	36.4	< 0.001
Thaw stage	2	18.1	17.1	< 0.001
Depth x Thaw stage	4	22.1	0.9	0.458

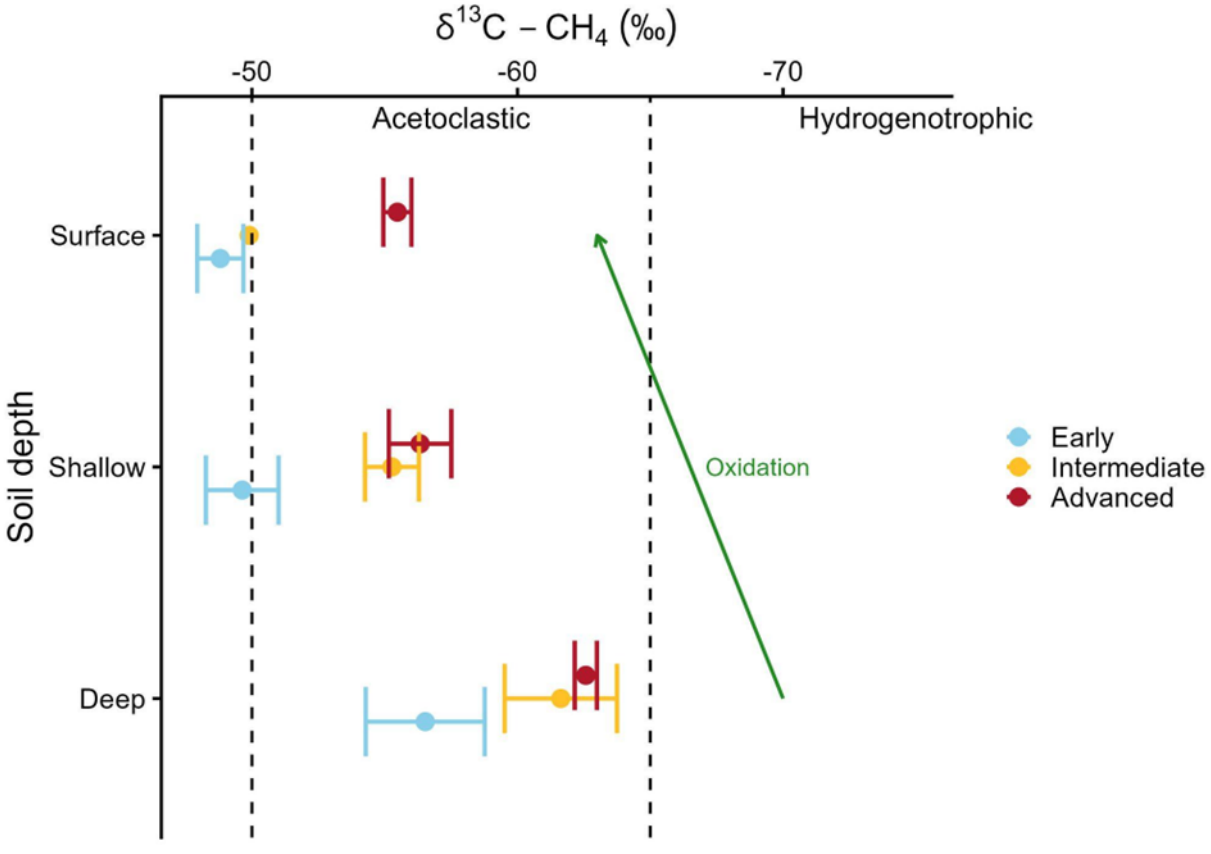

Figure 4. Mean $\delta^{13}C$-CH_4 values with depth and across thaw stages (early, intermediate, and advanced). Stable plots were excluded due to the limited number of isotopic measurements available (n = 2). Surface measurements were collected from chamber headspace samples, while shallow (33 cm) and deep (depth to frost layer up to 100 cm) samples were obtained from

https://doi.org/10.5194/egusphere-2026-2809
Preprint. Discussion started: 6 July 2026

porewater gas. The green arrow represents how we would expect increased CH_4 oxidation to alter $\delta^{13}C$-CH_4 values. Points represent means and error bars indicate ± 1 SE.

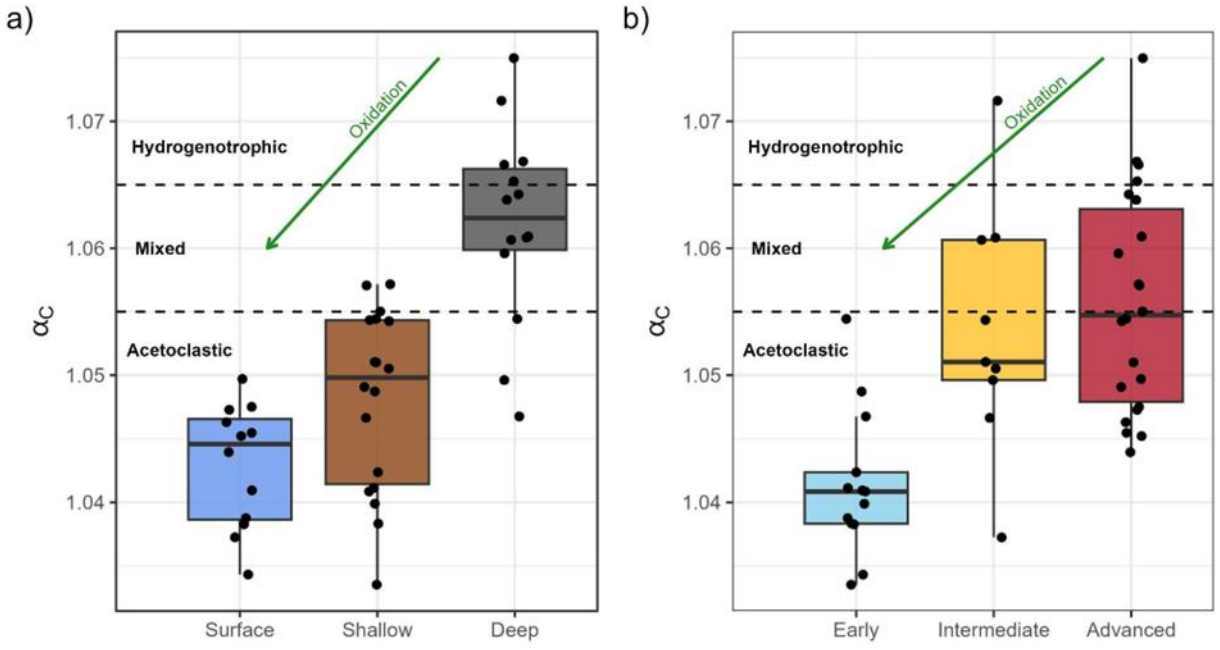

Figure 5. Carbon isotope fractionation factor (α_C) across **a)** soil depths (surface, shallow, and deep) and **b)** thaw stages (early, intermediate, and advanced). Dashed horizontal lines indicate commonly accepted thresholds separating dominant methanogenic pathways. The green arrow represents how we would expect increased CH_4 oxidation to alter fractionation factors. Stable plots were excluded due to the limited number of isotopic measurements available (n = 2).

Using the Rayleigh fractionation model, we estimated the percent of CH_4 oxidized during transport from deep porewater to surface fluxes. Only two early-thaw plots had both a deep porewater and chamber isotope measurement, so oxidation estimates were only calculated for intermediate and advanced thaw plots. Based on this model, approximately 40% of CH_4 produced at depth was oxidized before atmospheric release in the active thaw margin.

3.4 Microbial community composition

3.4.1 16S rRNA shifts along the thaw gradient

After quality filtering, 62 samples were retained for analysis. Samples were rarefied to 3,635 reads per sample, resulting in 11,421 unique ASVs across the dataset. Neither Shannon diversity ($p = 0.34$) nor taxonomic richness ($p = 0.70$) varied along the thaw gradient. Microbial community composition differed across thaw stages (PERMANOVA, $R^2 = 0.20$, $p = 0.001$). Pairwise comparisons showed that stable and early thaw stages did not differ ($p = 0.237$), but both were distinct from

https://doi.org/10.5194/egusphere-2026-2809
Preprint. Discussion started: 6 July 2026

intermediate and advanced stages (all $p \leq 0.006$). Soil depth also impacted community structure ($R^2 = 0.13$, $p = 0.001$), with a significant thaw stage x depth interaction ($R^2 = 0.10$, $p = 0.005$) indicating that thaw progression altered vertical community structure. Depth effects were significant across all thaw stages, but the greatest vertical differences were observed in intermediate thaw ($R^2 = 0.44$, $p = 0.018$). Tests for homogeneity of dispersion were not significant, indicating that differences among communities reflect shifts in community centroids in ordination space rather than increases in within-group variability.

Non-metric multidimensional scaling (NMDS) ordination (stress = 0.10) revealed clear clustering of microbial communities along the thaw gradient (Figure 6). Water table depth ($R^2 = 0.75$, $p = 0.001$), seasonal thaw depth ($R^2 = 0.72$, $p = 0.001$), and soil temperature ($R^2 = 0.57$, $p = 0.001$) were strongly associated with community structure (envfit). Methane flux ($R^2 = 0.23$, $p = 0.018$) and mean δ^{13}C-CH_4 ($R^2 = 0.46$, $p = 0.001$) were also correlated with community composition. Distance-based redundancy analysis identified seasonal thaw depth and water table depth as primary predictors of microbial structure, together explaining 29% of community variation.

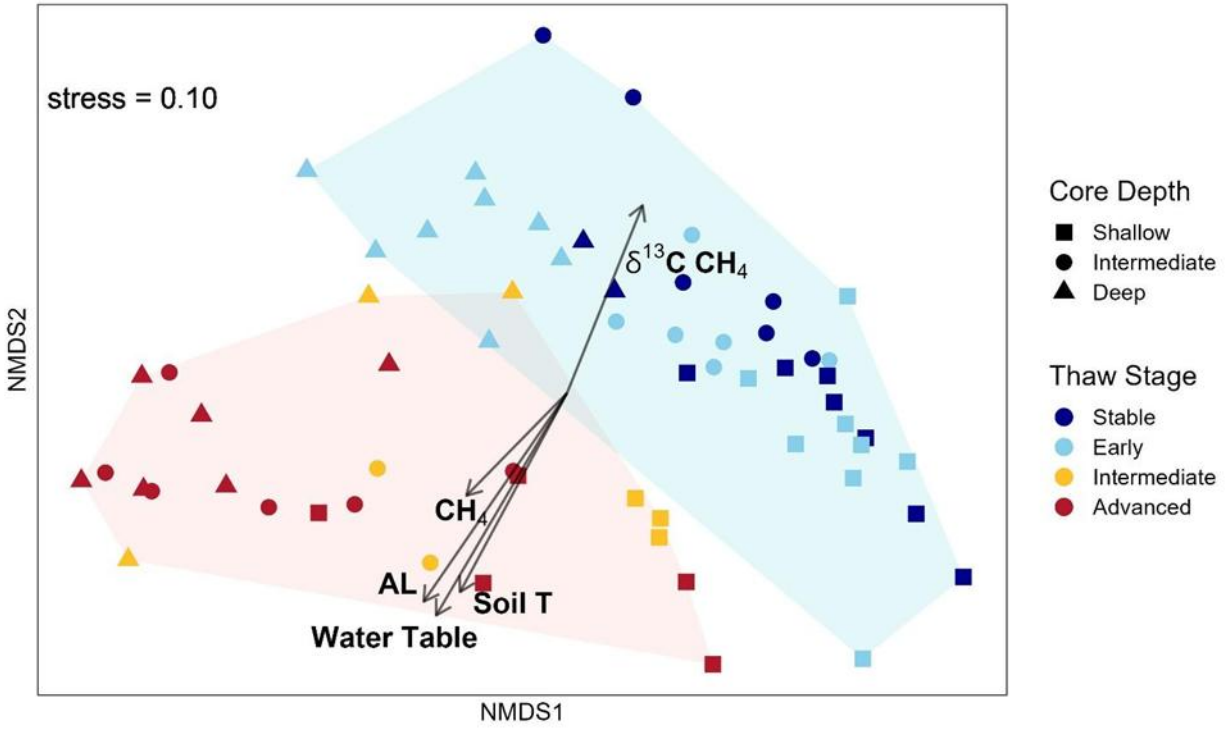

Figure 6. NMDS ordination of 16S rRNA gene community composition based on Bray-Curtis dissimilarity (stress = 0.1). Points represent individual samples, blue and red hulls represent the permafrost plateau (blue) and the active thaw margin (red), shapes represent core depth, and colored points represent thaw stage. Vectors indicate variables significantly correlated with community composition (envfit, $p < 0.05$): Soil T = soil temperature, AL = seasonal thaw depth, and Water Table = water table depth.

https://doi.org/10.5194/egusphere-2026-2809
Preprint. Discussion started: 6 July 2026

Several dominant bacterial phyla shifted along the thaw gradient (Figure 7). Acidobacteriota, Actinobacteriota, and Pseudomonadota declined in relative abundance while Chloroflexi and Bacteroidota increased substantially as thaw progressed ($p < 0.001$), with Bacteroidota exhibiting more than a tenfold increase in relative abundance from stable to advanced thaw stages. Euryarchaeota (which includes some methanogenic taxa) also increased along the thaw gradient ($p < 0.001$).

Functional guild analyses also showed that thaw progression increased total methanogen abundance ($p < 0.001$). This increase was primarily driven by hydrogenotrophic ($p < 0.001$) and mixotrophic ($p < 0.001$) methanogens while acetoclastic ($p = 0.14$) and methyl-based ($p = 0.59$) guilds were largely unaffected by thaw. Most methanogen guilds showed increased abundance at depth ($p \leq 0.01$) except for hydrogenotrophic methanogens, which did not vary with depth ($p = 0.09$). Total methanogen abundance was positively associated with CH_4 flux, explaining 21 % of the observed variation ($R^2 = 0.21$, $p < 0.001$). When including thaw stage as a predictor variable, the model accounted for 76 % of variation in CH_4 flux ($p < 0.001$).

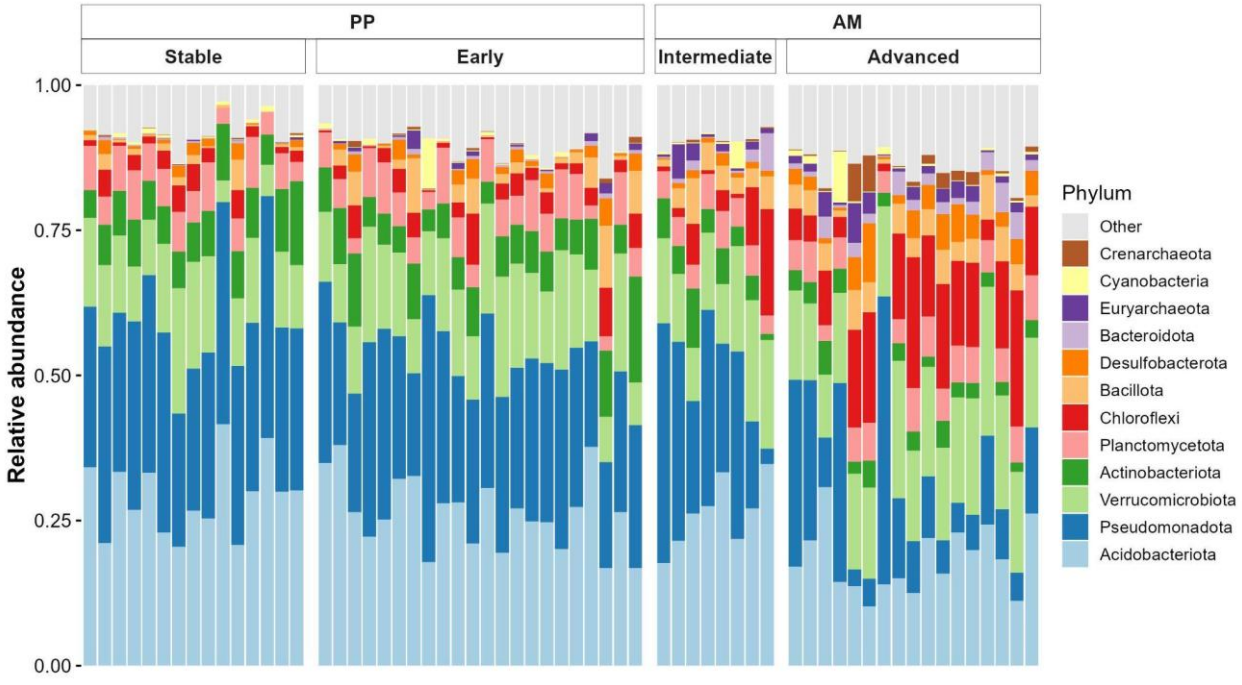

Figure 7. Phylum-level community composition across soil cores spanning the permafrost plateau (PP) and active thaw margin (AM) thaw gradient. Stacked bars show relative abundance per core, colored by taxonomic phylum. Shown are the top 12 phyla, with all other phyla aggregated into the "Other" category. Phyla are sorted from bottom to top based on average relative abundance across all samples.

https://doi.org/10.5194/egusphere-2026-2809
Preprint. Discussion started: 6 July 2026

3.4.2 mcrA shifts along the thaw gradient

After quality filtering and rarefying to 4,498 reads per sample, the mcrA dataset had 1,481 ASVs across 80 samples. Methanogen alpha-diversity varied significantly along the thaw gradient (Shannon $p < 0.001$; richness $p = 0.005$) with a significant thaw stage x depth interaction ($p < 0.001$). Core depth alone did not influence either alpha-diversity metric ($p > 0.05$). Both Shannon diversity and ASV richness declined from stable to intermediate thaw but increased substantially in advanced thaw plots, which had the highest overall diversity and elevated diversity across all depths.

Methanogen community composition varied across thaw stages (PERMANOVA, $R^2 = 0.3$, $p = 0.001$), with additional contributions from core depth ($R^2 = 0.06$, $p = 0.001$) and a thaw stage x depth interaction ($R^2 = 0.08$, $p = 0.009$), indicating depth-dependent restructuring of communities. Thaw stage and depth explained 44% of compositional variation. Multivariate dispersion did not differ among thaw stages ($p = 0.12$), confirming that differences reflected shifts in community structure rather than dispersion.

NMDS ordination (Bray-Curtis; stress = 0.1) revealed clear clustering of methanogen communities along the thaw gradient (Figure 8). Similar to the 16S rRNA gene sequencing results, the stable and early thaw samples clustered together; however, the mcrA sequencing results showed differences between intermediate and advanced thaw samples, unlike the 16S rRNA gene data. Seasonal thaw depth ($R^2 = 0.74$, $p = 0.001$), water table depth ($R^2 = 0.65$, $p = 0.001$), mean $\delta^{13}C\text{-}CH_4$ ($R^2 = 0.56$, $p = 0.001$), soil temperature ($R^2 = 0.48$, $p = 0.001$), CH_4 flux ($R^2 = 0.39$, $p = 0.001$), and CO_2 flux ($R^2 = 0.25$, $p = 0.002$) were significant correlates of community composition (envfit). When environmental variables were evaluated using redundancy analysis, seasonal thaw depth alone emerged as the best predictor, accounting for 18.6% of total community variation ($p = 0.001$).

https://doi.org/10.5194/egusphere-2026-2809
Preprint. Discussion started: 6 July 2026

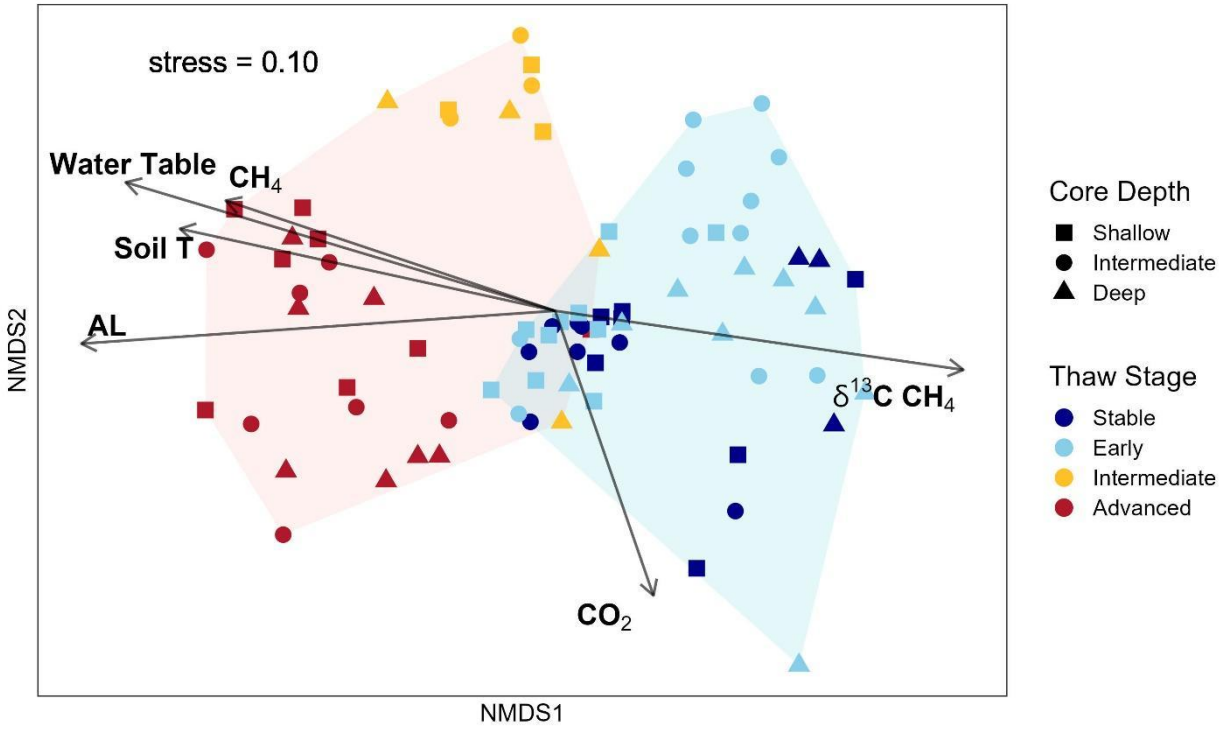

Figure 8. NMDS ordination of mcrA gene community composition based on Bray-Curtis dissimilarity (stress = 0.1). Points represent individual samples, blue and red hulls represent the permafrost plateau (blue) and the active thaw margin (red), shapes represent core depth, and colored points represent thaw stage. Vectors indicate variables significantly correlated with community composition (envfit, $p < 0.05$): Soil T = soil temperature, AL = seasonal thaw depth, and Water Table = water table depth.

Across all samples, methanogen communities were strongly dominated by hydrogenotrophic taxa, particularly *Methanobacterium*, which made up 73 % of total relative abundance (Figure 9). However, thaw progression substantially altered composition. *Methanobacterium* declined with thaw ($p < 0.001$), decreasing from ~78-89 % abundance in stable and early thaw stage to ~56-64 % abundance in advanced thaw, with the strong declines observed in deep soils.

In contrast, *Methanoregula* (hydrogenotrophs) greatly increased along the thaw gradient ($p < 0.001$). *Methanoregula* was rare in stable thaw stage and nearly absent in stable deep soils but expanded substantially in intermediate and advanced thaw, particularly at depth, reaching high relative abundance throughout the soil profile in advanced plots. The rapid expansion of *Methanoregula* explained 36% of CH_4 emissions but only 17% of δ^{13}C-CH_4 variation. *Methanosarcina* (mixotrophs) showed a moderate increase in intermediate thaw ($p = 0.055$), especially in intermediate and deep soils, while the acetoclastic genus

https://doi.org/10.5194/egusphere-2026-2809
Preprint. Discussion started: 6 July 2026

Methanothrix remained low overall and did not vary significantly across thaw stages, though its highest relative abundance occurred in advanced deep soils.

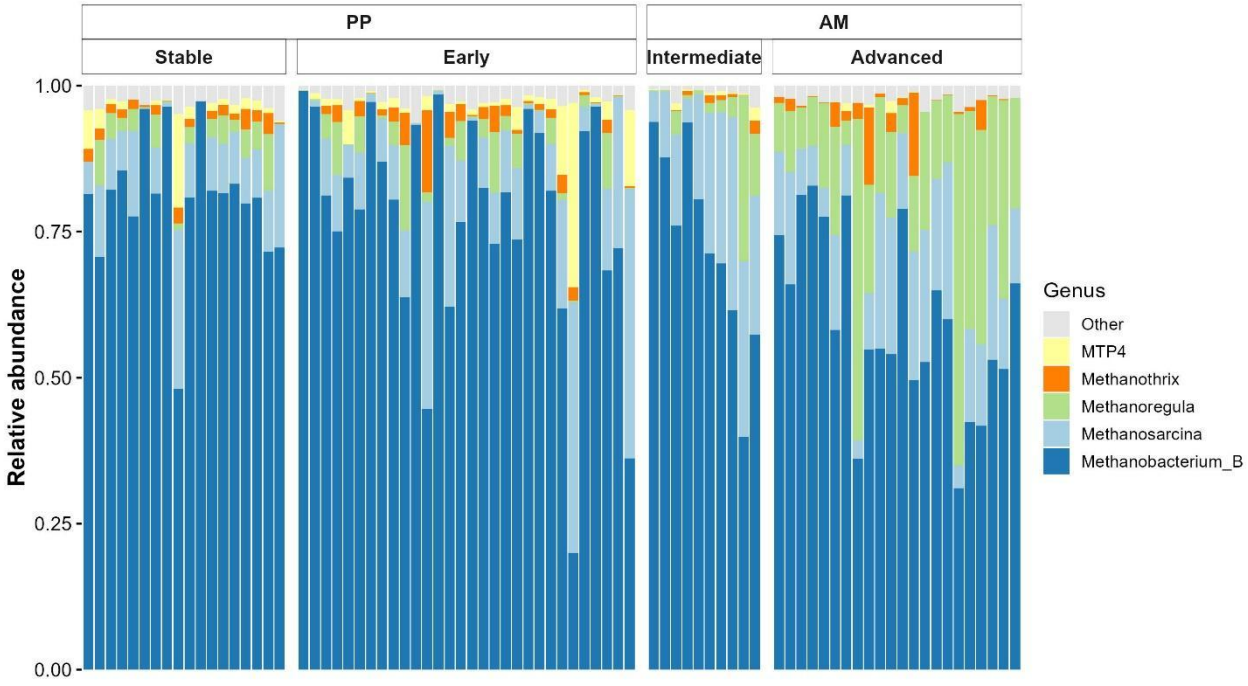

Figure 9. Genus-level community composition of mcrA sequences across soil cores spanning the permafrost plateau (PP) and active thaw margin (AM) thaw gradient. Stacked bars show relative abundance per core with the five most abundant genera shown individually and remaining taxa grouped as "Other".

4. Discussion

4.1 Thaw-driven environmental change restructures carbon processing

Permafrost thaw altered both environmental conditions and carbon fluxes. The disproportionate increase in CH_4 fluxes compared to CO_2 supports similar patterns from other peatlands (Heffernan et al., 2022; Malhotra and Roulet, 2015; Turetsky et al., 2002) and reflects long term observations from the site. These biogeochemical shifts coincided with rising water tables, warmer soil temperatures, and thicker seasonal thaw depths (Figure 2). Elevated water tables likely diminished oxygen availability and expanded anoxic microsites (Kettunen, 2003), while warming enhanced microbial metabolic rates and substrate release (Walker et al., 2018; Xu et al., 2023). Supporting this interpretation, Bacteroidota increased more than tenfold from stable to advanced thaw stages (Figure 7) and are known degraders of complex plant-derived organic matter including polysaccharides such as cellulose through diverse carbohydrate-active enzyme systems and polysaccharide utilization loci (Pan

https://doi.org/10.5194/egusphere-2026-2809
Preprint. Discussion started: 6 July 2026

et al., 2023; Lapébie et al., 2019). This indicates enhanced potential for the initial depolymerization of soil organic carbon under thawed conditions which likely increased H_2 availability from substrate fermentation, giving hydrogenotrophic taxa a competitive advantage (Philben et al., 2020; Wilmoth et al., 2021).

The large increase in CH_4 emissions without corresponding changes in CO_2 (Figure 3) indicates that permafrost thaw is altering the balance of carbon loss pathways rather than uniformly increasing ecosystem respiration. This is consistent with eddy covariance flux measurements showing that our study site is a small CO_2 source (annual data) but a much larger CH_4 source based on April-October measurements (Euskirchen et al., 2024). Similar trends have been observed at other high-latitude peatlands where permafrost thaw leads to rising water tables (Euskirchen et al., 2014; Moore and Dalva, 1993; Turetsky et al., 2002; Yu et al., 2017). Advanced thaw CH_4 fluxes were consistently higher than the rest of the thaw gradient, and often exceed reported flux measurements from other permafrost peatlands (Chen et al., 2025; Heffernan et al., 2022; Natali et al., 2015). Due to the high radiative forcing of CH_4 compared to CO_2, even small increases in CH_4 emissions could offset increases in CO_2 uptake, shifting these ecosystems toward a net positive radiative forcing. Resolving the underlying mechanisms driving enhanced CH_4 production requires linking these environmental changes to microbial communities, particularly the restructuring of methanogens and methanotrophs.

4.2 Permafrost thaw functionally restructures methanogen communities

Permafrost thaw instigated a clear functional reorganization of methanogen communities. As thaw progressed from stable permafrost to advanced thaw stages, *Methanoregula* (hydrogenotroph) increased dramatically in relative abundance (Figure 9), with the strongest signal observed at depth but with consistent shifts throughout the soil profile. *Methanoregula* is an obligate anaerobe that thrives in low pH environments (4.5-5.5) and is adapted to oligotrophic environments (Bräuer et al., 2011). To our knowledge, no studies to date have quantified CH_4 production rates from *Methanoregula* isolates, and *Methanoregula* has rarely been emphasized in permafrost peatland research. However, *Methanoregula* has been identified as a dominant methanogen in high CH_4-emitting wetlands and found to be significantly correlated with CH_4 flux (Bechtold et al., 2025). Genomic evidence further suggests that some *Methanoregula* may have methylotrophic potential (Bechtold et al., 2025), indicating that this CH_4 production pathway may play a bigger role in these ecosystems than previously recognized. The strong association between *Methanoregula* abundance and CH_4 emissions suggests that this taxon plays a strong role in regulating CH_4 output under thawing conditions, although isotopic variation indicates additional controls beyond production pathway alone.

As *Methanoregula* relative abundance increased along the thaw gradient, *Methanobacterium*, the most abundant genus across all thaw stages, declined (Figure 9). *Methanobacterium* is an anaerobic, mesophilic, and hydrogentrophic methanogen that prefers neutral pH conditions (range: 5.0-8.5) (Enzmann et al., 2018; Trubitsyn et al., 2023). The negative correlation between these two methanogens suggests increased competition among hydrogenotrophic methanogens as permafrost thaw progresses.

https://doi.org/10.5194/egusphere-2026-2809
Preprint. Discussion started: 6 July 2026

Methanothrix (an obligate acetoclastic methanogen in the Methanotrichaceae family) and *Methanosarcina* (a mixotroph in the Methanosarcinaceae family) did not vary across thaw stages, suggesting that acetate availability did not increase with thaw progression and/or that acidic peat bog conditions constrained acetoclastic methanogenesis.

While some studies have reported increased acetoclastic methanogenesis with thaw (Heffernan et al., 2022; McCalley et al., 2014), our findings support studies showing enhanced hydrogenotrophic methanogenesis (Holm et al., 2020; Liebner et al., 2015). Thaw appears to favor methanogenic taxa adapted to H_2/CO_2 substrates, fundamentally altering the metabolic mechanism of CH_4 production.

4.3 Methane oxidation decouples isotopic signatures from methanogenic pathways

Even though δ^{13}C-CH_4 values became more depleted with thaw progression, suggesting increasing hydrogenotrophic influence, the apparent fractionation values of all CH_4 fluxes fall within ranges typical of acetoclastic methanogenesis (Figure 5). However, methanogen taxonomic data showed no increases in acetoclastic potential across the thaw gradient since *Methanothrix* and *Methanosarcina* relative abundances remained stable. Acetoclastic inputs cannot be ruled out, but the most pronounced shift from stable to advanced thaw was increased hydrogenotrophic dominance driven by *Methanoregula* (Figure 9).

Although functional gene abundance or activity was not directly quantified, the combination of enriched isotopic values and methanotroph community presence across all thaw stages supports that oxidation significantly modified emitted CH_4 isotopic signatures (Templeton et al., 2006; Wang et al., 2016). Our results support this mechanism in the active thaw margin, with an estimated 40% of CH_4 produced at depth being oxidized before reaching the atmosphere. Although this oxidation rate is slightly lower than reported averages from other peatlands (Nielsen et al., 2018; Smemo and Yavitt, 2011; Yavitt et al., 1988), it still represents a substantial CH_4 sink and meaningful alteration of the emitted isotopic signature.

Previous work at this site has also shown that CH_4 production exceeds oxidation rates and vascular plant presence (particularly sedges) suppresses CH_4 oxidation (Neumann et al., 2016; Turner et al., 2020). These findings support our observation that production strongly outweighed oxidation, and that advanced thaw plots, which are characterized by greater vascular plant abundance, likely experienced reduced oxidation.

By integrating CH_4 fluxes, isotopic composition, and microbial community structure, we show that CH_4 oxidation alters the signature of emitted CH_4. If only CH_4 fluxes and isotopic values are measured, ^{13}C enrichment caused by CH_4 oxidation could be misinterpreted as evidence for acetoclastic methanogenesis even when hydrogenotrophic taxa dominate. Alternatively, only considering microbial data could suggest more depleted CH_4 emissions, ignoring carbon enrichment during oxidation in

https://doi.org/10.5194/egusphere-2026-2809
Preprint. Discussion started: 6 July 2026

surface soils. Consequently, relying solely on isotopic values may misrepresent methanogenic pathways and mask the true mechanisms driving carbon loss under permafrost thaw.

5. Conclusion

Our study showed that permafrost thaw caused wetting, deeper seasonal thaw, increased CH_4 emissions, and induced widespread expansion of methanogens. Increased hydrogenotrophs (particularly *Methanoregula*) along the thaw gradient suggests that thaw promotes conditions favorable for metabolism of H_2 and CO_2. However, isotopic enrichment of emitted CH_4 and Rayleigh fractionation modeling indicate that substantial CH_4 oxidation occurred before CH_4 reached the atmosphere, obscuring the underlying production pathways. Our findings demonstrate that identifying CH_4 production pathways based on isotopic signatures alone may conceal the true microbial mechanisms driving carbon cycling in these systems. Therefore, integrating fluxes, isotopes, and microbial community structure is necessary to accurately characterize CH_4 dynamics and predict permafrost carbon feedbacks in rapidly thawing permafrost peatlands.

Code and data availability

All code and data used in this study are publicly available in the GitHub repository: https://github.com/ArcticWebb/APEX_Beta.

Author contributions

HW, CD, SKS, and MEM designed the experiment and developed protocols for field sampling, sample storage, and subsequent analyses. HW led labwork with assistance from AS and MEM. CPBM and MEM assisted HW with bioinformatics and downstream statistical analyses. HW drafted the manuscript with contributions from all coauthors.

Competing interests

The authors declare no competing interests.

Disclaimer

Any errors and opinions are not those of the Army Research Office or Department of Defense and are attributable solely to the authors. Any opinions, findings, conclusions, or recommendations expressed in the material are those of the author(s) and do not necessarily reflect the views of the National Science Foundation.

https://doi.org/10.5194/egusphere-2026-2809
Preprint. Discussion started: 6 July 2026

Acknowledgements

We thank Jesse Rush and Breena Lijewski for their assistance with field data collection. We also acknowledge the Bonanza Creek Long-Term Ecology Research Program and its staff for providing vehicles, equipment, site access, and logistical support throughout this project. This work utilized the Alpine high performance computing resource at the University of Colorado Boulder. Alpine is jointly funded by the University of Colorado Boulder, the University of Colorado Anschutz, Colorado State University, and the National Science Foundation (award #2201538).

Financial support

The research reported here was funded in whole or in part by the Army Research Office/Army Research Laboratory via grant #W911-NF-23-1-0311 to the University of Colorado. MEM was supported, in part, by the National Science Foundation award #2311074. This material is based upon work supported by the National Science Foundation under grant #1929393. Isotope analysis was supported by the National Science Foundation (award #2411998).

References

Anderson, M. J.: Distance-based tests for homogeneity of multivariate dispersions, biometrics, 62, 245–253, https://doi.org/10.1111/j.1541-0420.2005.00440.x, 2006.

Apprill, A., McNally, S., Parsons, R., and Weber, L.: Minor revision to V4 region SSU rRNA 806R gene primer greatly increases detection of SAR11 bacterioplankton, Aquat. Microb. Ecol., 75, 129–137, https://doi.org/10.3354/ame01753, 2015.

Bäck, H., May, R., Naidu, D. S., and Eikenberry, S.: Effect of methane mitigation on global temperature under a permafrost feedback, Glob. Environ. Change Adv., 2, 100005, https://doi.org/10.1016/j.gecadv.2024.100005, 2024.

Bechtold, E. K., Ellenbogen, J. B., Villa, J. A., De Melo Ferreira, D. K., Oliverio, A. M., Kostka, J. E., Rich, V. I., Varner, R. K., Bansal, S., Ward, E. J., Bohrer, G., Borton, M. A., Wrighton, K. C., and Wilkins, M. J.: Metabolic interactions underpinning high methane fluxes across terrestrial freshwater wetlands, Nat. Commun., 16, 944, https://doi.org/10.1038/s41467-025-56133-0, 2025.

Bräuer, S. L., Cadillo-Quiroz, H., Ward, R. J., Yavitt, J. B., and Zinder, S. H.: *Methanoregula boonei* gen. nov., sp. nov., an acidiphilic methanogen isolated from an acidic peat bog, Int. J. Syst. Evol. Microbiol., 61, 45–52, https://doi.org/10.1099/ijs.0.021782-0, 2011.

Bueno de Mesquita, C. P., Wu, D., and Tringe, S. G.: Methyl-based methanogenesis: an ecological and genomic review, Microbiol. Mol. Biol. Rev., 87, e00024-22, https://doi.org/10.1128/mmbr.00024-22, 2023.

Burke, E. J., Hartley, I. P., and Jones, C. D.: Uncertainties in the global temperature change caused by carbon release from permafrost thawing, The Cryosphere, 6, 1063–1076, https://doi.org/10.5194/tc-6-1063-2012, 2012.

https://doi.org/10.5194/egusphere-2026-2809
Preprint. Discussion started: 6 July 2026

Camacho, C., Coulouris, G., Avagyan, V., Ma, N., Papadopoulos, J., Bealer, K., and Madden, T. L.: BLAST+: architecture and applications, BMC Bioinformatics, 10, 421, https://doi.org/10.1186/1471-2105-10-421, 2009.

Chapin, F. S., Oswood, M. W., van Cleve, K., Viereck, L. A., and Verbyla, D. L.: Alaska's changing boreal forest, Oxford University Press, 2006.

Chasar, L. S., Chanton, J. P., Glaser, P. H., Siegel, D. I., and Rivers, J. S.: Radiocarbon and stable carbon isotopic evidence for transport and transformation of dissolved organic carbon, dissolved inorganic carbon, and CH_4 in a northern Minnesota peatland, Glob. Biogeochem. Cycles, 14, 1095–1108, https://doi.org/10.1029/1999GB001221, 2000.

Chen, H., Bittner, D., Yin, W., Thompson, L., Campbell, G., Hastings, A., and Abdalla, M.: Dynamics of methane flux in permafrost-affected wetlands: A meta-analysis of permafrost continuity effects and hydrological controls, Environ. Pollut., 385, 127040, https://doi.org/10.1016/j.envpol.2025.127040, 2025.

Chen, Y., Liu, F., Kang, L., Zhang, D., Kou, D., Mao, C., Qin, S., Zhang, Q., and Yang, Y.: Large-scale evidence for microbial response and associated carbon release after permafrost thaw, Glob. Change Biol., 27, 3218–3229, https://doi.org/10.1111/gcb.15487, 2021.

Chuvochina, M., Gerken, J., Frentrup, M., Sandikci, Y., Goldmann, R., Freese, H. M., Göker, M., Sikorski, J., Yarza, P., Quast, C., Peplies, J., Glöckner, F. O., and Reimer, L. C.: SILVA in 2026: a global core biodata resource for rRNA within the DSMZ digital diversity, Nucleic Acids Res., 54, D334–D341, https://doi.org/10.1093/nar/gkaf1247, 2026.

Clark, I. and Fritz, P.: Environmental isotopes in hydrology, Lewis Publ., 1998.

Corbett, J. E., Tfaily, M. M., Burdige, D. J., Cooper, W. T., Glaser, P. H., and Chanton, J. P.: Partitioning pathways of CO2 production in peatlands with stable carbon isotopes, Biogeochemistry, 114, 327–340, https://doi.org/10.1007/s10533-012-9813-1, 2013.

Cox, W. D., Dieleman, C. M., Douglas, T. A., Kane, E. S., Neumann, R. B., Euskirchen, E. S., and Turetsky, M. R.: Plant community shifts as early indicators of abrupt permafrost thaw and associated carbon release in an interior Alaskan peatland, J. Geophys. Res. Biogeosciences, 130, e2024JG008639, https://doi.org/10.1029/2024JG008639, 2025.

Enzmann, F., Mayer, F., Rother, M., and Holtmann, D.: Methanogens: biochemical background and biotechnological applications, AMB Expr, 8, 1, https://doi.org/10.1186/s13568-017-0531-x, 2018.

Euskirchen, E. S., Edgar, C. W., Turetsky, M. R., Waldrop, M. P., and Harden, J. W.: Differential response of carbon fluxes to climate in three peatland ecosystems that vary in the presence and stability of permafrost: Carbon fluxes and permafrost thaw, J. Geophys. Res. Biogeosciences, 119, 1576–1595, https://doi.org/10.1002/2014JG002683, 2014.

Euskirchen, E. S., Edgar, C. W., Kane, E. S., Waldrop, M. P., Neumann, R. B., Manies, K. L., Douglas, T. A., Dieleman, C., Jones, M. C., and Turetsky, M. R.: Persistent net release of carbon dioxide and methane from an Alaskan lowland boreal peatland complex, Glob. Change Biol., 30, e17139, https://doi.org/10.1111/gcb.17139, 2024.

Glenn, T. C., Pierson, T. W., Bayona-Vásquez, N. J., Kieran, T. J., Hoffberg, S. L., Thomas Iv, J. C., Lefever, D. E., Finger, J. W., Gao, B., Bian, X., Louha, S., Kolli, R. T., Bentley, K. E., Rushmore, J., Wong, K., Shaw, T. I., Rothrock Jr, M. J., McKee, A. M., Guo, T. L., Mauricio, R., Molina, M., Cummings, B. S., Lash, L. H., Lu, K., Gilbert, G. S., Hubbell, S. P., and

https://doi.org/10.5194/egusphere-2026-2809
Preprint. Discussion started: 6 July 2026

Faircloth, B. C.: Adapterama II: universal amplicon sequencing on Illumina platforms (TaggiMatrix), PeerJ, 7, e7786, https://doi.org/10.7717/peerj.7786, 2019.

Hansen, L. V., Tariq, A., Jensen, L. S., and Bruun, S.: Using weather forecasts to avoid major emission events of N2O in connection with manure application, Agric. Water Manag., 318, 109689, https://doi.org/10.1016/j.agwat.2025.109689, 2025.

Harris, L. I., Richardson, K., Bona, K. A., Davidson, S. J., Finkelstein, S. A., Garneau, M., McLaughlin, J., Nwaishi, F., Olefeldt, D., Packalen, M., Roulet, N. T., Southee, F. M., Strack, M., Webster, K. L., Wilkinson, S. L., and Ray, J. C.: The essential carbon service provided by northern peatlands, Front. Ecol. Environ., 20, 222–230, https://doi.org/10.1002/fee.2437, 2022.

Hartman, W. H., Bueno De Mesquita, C. P., Theroux, S. M., Morgan-Lang, C., Baldocchi, D. D., and Tringe, S. G.: Multiple microbial guilds mediate soil methane cycling along a wetland salinity gradient, mSystems, 9, e00936-23, https://doi.org/10.1128/msystems.00936-23, 2024.

Heffernan, L., Cavaco, M. A., Bhatia, M. P., Estop-Aragonés, C., Knorr, K.-H., and Olefeldt, D.: High peatland methane emissions following permafrost thaw: enhanced acetoclastic methanogenesis during early successional stages, Biogeosciences, 19, 3051–3071, https://doi.org/10.5194/bg-19-3051-2022, 2022.

Helbig, M., Živković, T., Alekseychik, P., Aurela, M., El-Madany, T. S., Euskirchen, E. S., Flanagan, L. B., Griffis, T. J., Hanson, P. J., Hattakka, J., Helfter, C., Hirano, T., Humphreys, E. R., Kiely, G., Kolka, R. K., Laurila, T., Leahy, P. G., Lohila, A., Mammarella, I., Nilsson, M. B., Panov, A., Parmentier, F. J. W., Peichl, M., Rinne, J., Roman, D. T., Sonnentag, O., Tuittila, E.-S., Ueyama, M., Vesala, T., Vestin, P., Weldon, S., Weslien, P., and Zaehle, S.: Warming response of peatland CO2 sink is sensitive to seasonality in warming trends, Nat. Clim. Change, 12, 743–749, https://doi.org/10.1038/s41558-022-01428-z, 2022.

Hervé, M.: RVAideMemoire: Testing and plotting procedures for biostatistics (R package version 0.9-83-12), 2025.

Holm, S., Walz, J., Horn, F., Yang, S., Grigoriev, M. N., Wagner, D., Knoblauch, C., and Liebner, S.: Methanogenic response to long-term permafrost thaw is determined by paleoenvironment, FEMS Microbiol. Ecol., 96, fiaa021, https://doi.org/10.1093/femsec/fiaa021, 2020.

Horn, M. A., Matthies, C., Küsel, K., Schramm, A., and Drake, H. L.: Hydrogenotrophic methanogenesis by moderately acid-tolerant methanogens of a methane-emitting acidic peat, Appl. Environ. Microbiol., 69, 74–83, https://doi.org/10.1128/AEM.69.1.74-83.2003, 2003.

Hornibrook, E. R. C., Longstaffe, F. J., and Fyfe, W. S.: Evolution of stable carbon isotope compositions for methane and carbon dioxide in freshwater wetlands and other anaerobic environments, Geochim. Cosmochim. Acta, 64, 1013–1027, https://doi.org/10.1016/S0016-7037(99)00321-X, 2000.

Hugelius, G., Strauss, J., Zubrzycki, S., Harden, J. W., Schuur, E. A. G., Ping, C.-L., Schirrmeister, L., Grosse, G., Michaelson, G. J., Koven, C. D., O'Donnell, J. A., Elberling, B., Mishra, U., Camill, P., Yu, Z., Palmtag, J., and Kuhry, P.: Estimated stocks of circumpolar permafrost carbon with quantified uncertainty ranges and identified data gaps, Biogeosciences, 11, 6573–6593, https://doi.org/10.5194/bg-11-6573-2014, 2014.

https://doi.org/10.5194/egusphere-2026-2809
Preprint. Discussion started: 6 July 2026

Jorgenson, M. T., Kanevskiy, M., Roland, C., Hill, K., Schirokauer, D., Stehn, S., Schroeder, B., and Shur, Y.: Repeated permafrost formation and degradation in boreal peatland ecosystems in relation to climate extremes, fire, ecological shifts, and a geomorphic legacy, Atmosphere, 13, 1170, https://doi.org/10.3390/atmos13081170, 2022.

Kettunen, A.: Connecting methane fluxes to vegetation cover and water table fluctuations at microsite level: A modeling study, Glob. Biogeochem. Cycles, 17, 2002GB001958, https://doi.org/10.1029/2002GB001958, 2003.

King, G. M.: Regulation by light of methane emissions from a wetland, Nature, 345, 513–515, https://doi.org/10.1038/345513a0, 1990.

Klaus, M., Öquist, M., and Macháčová, K.: Tree stem-atmosphere greenhouse gas fluxes in a boreal riparian forest, Sci. Total Environ., 954, 176243, https://doi.org/10.1016/j.scitotenv.2024.176243, 2024.

Knoblauch, C., Beer, C., Liebner, S., Grigoriev, M. N., and Pfeiffer, E.-M.: Methane production as key to the greenhouse gas budget of thawing permafrost, Nat. Clim. Change, 8, 309–312, https://doi.org/10.1038/s41558-018-0095-z, 2018.

Kuhn, M. A., Varner, R. K., McCalley, C. K., Perryman, C. R., Aurela, M., Burke, S. A., Chanton, J. P., Crill, P. M., DelGreco, J., Deng, J., Heffernan, L., Herrick, C., Hodgkins, S. B., Jones, C. P., Juutinen, S., Kane, E. S., Lamit, L. J., Larmola, T., Lilleskov, E., Olefeldt, D., Palace, M. W., Rich, V. I., Schulze, C., Shorter, J. H., Sullivan, F. B., Sonnentag, O., Turetsky, M. R., and Waldrop, M. P.: Controls on stable methane isotope values in northern peatlands and potential shifts in values under permafrost thaw scenarios, J. Geophys. Res. Biogeosciences, 129, e2023JG007837, https://doi.org/10.1029/2023JG007837, 2024.

Kuznetsova, A., Bruun Brockhoff, P., and Haubo Bojesen Christensen, R.: lmerTest: Tests in linear mixed effects models, https://doi.org/10.32614/CRAN.package.lmerTest, 2013.

Lapébie, P., Lombard, V., Drula, E., Terrapon, N., and Henrissat, B.: Bacteroidetes use thousands of enzyme combinations to break down glycans, Nat Commun, 10, 2043, https://doi.org/10.1038/s41467-019-10068-5, 2019.

Leff, J. W.: mctoolsr: Microbial community data analysis tools (0.1.1.9), 2022.

Legendre, P. and Legendre, L.: Numerical Ecology, Developments in environmental modeling, 3rd edition., Elsevier Amsterdam, 419 pp., 2012.

Liebner, S., Ganzert, L., Kiss, A., Yang, S., Wagner, D., and Svenning, M. M.: Shifts in methanogenic community composition and methane fluxes along the degradation of discontinuous permafrost, Front. Microbiol., 6, https://doi.org/10.3389/fmicb.2015.00356, 2015.

Malhotra, A. and Roulet, N. T.: Environmental correlates of peatland carbon fluxes in a thawing landscape: do transitional thaw stages matter?, Biogeosciences, 12, 3119–3130, https://doi.org/10.5194/bg-12-3119-2015, 2015.

Martin, M.: Cutadapt removes adapter sequences from high-throughput sequencing reads, EMBnet j., 17, 10, https://doi.org/10.14806/ej.17.1.200, 2011.

McCalley, C. K., Woodcroft, B. J., Hodgkins, S. B., Wehr, R. A., Kim, E.-H., Mondav, R., Crill, P. M., Chanton, J. P., Rich, V. I., Tyson, G. W., and Saleska, S. R.: Methane dynamics regulated by microbial community response to permafrost thaw, Nature, 514, 478–481, https://doi.org/10.1038/nature13798, 2014.

https://doi.org/10.5194/egusphere-2026-2809
Preprint. Discussion started: 6 July 2026

Moore, T. R. and Dalva, M.: The influence of temperature and water table position on carbon dioxide and methane emissions from laboratory columns of peatland soils, J. Soil Sci., 44, 651–664, https://doi.org/10.1111/j.1365-2389.1993.tb02330.x, 1993.

Natali, S. M., Schuur, E. A. G., Mauritz, M., Schade, J. D., Celis, G., Crummer, K. G., Johnston, C., Krapek, J., Pegoraro, E., Salmon, V. G., and Webb, E. E.: Permafrost thaw and soil moisture driving CO2 and CH4 release from upland tundra, J. Geophys. Res. Biogeosciences, 120, 525–537, https://doi.org/10.1002/2014JG002872, 2015.

Neumann, R. B., Blazewicz, S. J., Conaway, C. H., Turetsky, M. R., and Waldrop, M. P.: Modeling CH4 and CO2 cycling using porewater stable isotopes in a thermokarst bog in Interior Alaska: results from three conceptual reaction networks, Biogeochemistry, 127, 57–87, https://doi.org/10.1007/s10533-015-0168-2, 2016.

Nielsen, C. S., Hasselquist, N. J., Nilsson, M. B., Öquist, M., Järveoja, J., and Peichl, M.: A novel approach for high-frequency in-situ quantification of methane oxidation in peatlands, Soil Syst., 3, 4, https://doi.org/10.3390/soilsystems3010004, 2018.

NOAA National Centers for Environmental information: Climate at a glance: city time series, 2026.

Obu, J.: How much of the earth's surface is underlain by permafrost?, J. Geophys. Res. Earth Surf., 126, e2021JF006123, https://doi.org/10.1029/2021JF006123, 2021.

Oksanen, J., Simpson, G. L., Blanchet, F. G., Kindt, R., Legendre, P., Minchin, P. R., O'Hara, R. B., Solymos, P., Stevens, M. H. H., Szoecs, E., Wagner, H., Barbour, M., Bedward, M., Bolker, B., Borcard, D., Borman, T., Carvalho, G., Chirico, M., De Caceres, M., Durand, S., Evangelista, H. B. A., FitzJohn, R., Friendly, M., Furneaux, B., Hannigan, G., Hill, M. O., Lahti, L., Martino, C., McGlinn, D., Ouellette, M.-H., Ribeiro Cunha, E., Smith, T., Stier, A., Ter Braak, C. J. F., and Weedon, J.: vegan: community ecology package, https://doi.org/10.32614/CRAN.package.vegan, 2015.

Pan, X., Raaijmakers, J. M., and Carrión, V. J.: Importance of Bacteroidetes in host–microbe interactions and ecosystem functioning, Trends in Microbiology, 31, 959–971, https://doi.org/10.1016/j.tim.2023.03.018, 2023.

Parada, A. E., Needham, D. M., and Fuhrman, J. A.: Every base matters: assessing small subunit rRNA primers for marine microbiomes with mock communities, time series and global field samples, Environ. Microbiol., 18, 1403–1414, https://doi.org/10.1111/1462-2920.13023, 2016.

Parks, D. H., Chaumeil, P.-A., Mussig, A. J., Rinke, C., Chuvochina, M., and Hugenholtz, P.: GTDB release 10: a complete and systematic taxonomy for 715 230 bacterial and 17 245 archaeal genomes, Nucleic Acids Res., 54, D743–D754, https://doi.org/10.1093/nar/gkaf1040, 2026.

Penger, J., Conrad, R., and Blaser, M.: Stable carbon isotope fractionation by methylotrophic methanogenic archaea, Appl. Environ. Microbiol., 78, 7596–7602, https://doi.org/10.1128/AEM.01773-12, 2012.

Philben, M., Zhang, L., Yang, Z., Taş, N., Wullschleger, S. D., Graham, D. E., and Gu, B.: Anaerobic respiration pathways and response to increased substrate availability of Arctic wetland soils, Environ. Sci. Process. Impacts, 22, 2070–2083, https://doi.org/10.1039/D0EM00124D, 2020.

Qiu, C., Zhu, D., Ciais, P., Guenet, B., and Peng, S.: The role of northern peatlands in the global carbon cycle for the 21st century, Glob. Ecol. Biogeogr., 29, 956–973, https://doi.org/10.1111/geb.13081, 2020.

https://doi.org/10.5194/egusphere-2026-2809
Preprint. Discussion started: 6 July 2026

R Core Team: A language and environment for statistical computing. R foundation for statistical computing, 2025.

Rantanen, M., Karpechko, A. Yu., Lipponen, A., Nordling, K., Hyvärinen, O., Ruosteenoja, K., Vihma, T., and Laaksonen, A.: The Arctic has warmed nearly four times faster than the globe since 1979, Commun. Earth Environ., 3, 168, https://doi.org/10.1038/s43247-022-00498-3, 2022.

Salehnia, N., Park, C.-H., Park, H., Fedorov, N., Ahn, J., Fedorov, A., and Son, S.-W.: Positive surface air temperature trends in a subarctic region: Analyzing the changes in dominant periodic components and energy budget, Atmospheric Res., 318, 107981, https://doi.org/10.1016/j.atmosres.2025.107981, 2025.

Schloss, P. D.: Rarefaction is currently the best approach to control for uneven sequencing effort in amplicon sequence analyses, mSphere, 9, e00354-23, https://doi.org/10.1128/msphere.00354-23, 2024.

Schuur, E. A. G., Abbott, B. W., Commane, R., Ernakovich, J., Euskirchen, E., Hugelius, G., Grosse, G., Jones, M., Koven, C., Leshyk, V., Lawrence, D., Loranty, M. M., Mauritz, M., Olefeldt, D., Natali, S., Rodenhizer, H., Salmon, V., Schädel, C., Strauss, J., Treat, C., and Turetsky, M.: Permafrost and climate change: carbon cycle feedbacks from the warming Arctic, Annu. Rev. Environ. Resour., 47, 343–371, https://doi.org/10.1146/annurev-environ-012220-011847, 2022.

Smemo, K. A. and Yavitt, J. B.: Anaerobic oxidation of methane: an underappreciated aspect of methane cycling in peatland ecosystems?, Biogeosciences, 8, 779–793, https://doi.org/10.5194/bg-8-779-2011, 2011.

Swindles, G. T., Morris, P. J., Mullan, D., Watson, E. J., Turner, T. E., Roland, T. P., Amesbury, M. J., Kokfelt, U., Schoning, K., Pratte, S., Gallego-Sala, A., Charman, D. J., Sanderson, N., Garneau, M., Carrivick, J. L., Woulds, C., Holden, J., Parry, L., and Galloway, J. M.: The long-term fate of permafrost peatlands under rapid climate warming, Sci. Rep., 5, 17951, https://doi.org/10.1038/srep17951, 2015.

Templeton, A. S., Chu, K.-H., Alvarez-Cohen, L., and Conrad, M. E.: Variable carbon isotope fractionation expressed by aerobic CH4-oxidizing bacteria, Geochim. Cosmochim. Acta, 70, 1739–1752, https://doi.org/10.1016/j.gca.2005.12.002, 2006.

Trubitsyn, V. E., Suzina, N. E., Rivkina, E. M., and Shcherbakova, V. A.: A new methanogenic, hydrogenotrophic archaeon from Spitsbergen permafrost, Microbiology, 92, 119–128, https://doi.org/10.1134/S0026261722603256, 2023.

Turetsky, M. R., Wieder, R. K., and Vitt, D. H.: Boreal peatland C fluxes under varying permafrost regimes, Soil Biol. Biochem., 34, 907–912, https://doi.org/10.1016/S0038-0717(02)00022-6, 2002.

Turner, J. C., Moorberg, C. J., Wong, A., Shea, K., Waldrop, M. P., Turetsky, M. R., and Neumann, R. B.: Getting to the Root of Plant-Mediated Methane Emissions and Oxidation in a Thermokarst Bog, JGR Biogeosciences, 125, e2020JG005825, https://doi.org/10.1029/2020JG005825, 2020.

Waldrop, M. P., W. McFarland, J., Manies, K. L., Leewis, M. C., Blazewicz, S. J., Jones, M. C., Neumann, R. B., Keller, J. K., Cohen, L., Euskirchen, E. S., Edgar, C., Turetsky, M. R., and Cable, W. L.: Carbon fluxes and microbial activities from boreal peatlands experiencing permafrost thaw, J. Geophys. Res. Biogeosciences, 126, e2020JG005869, https://doi.org/10.1029/2020JG005869, 2021.

https://doi.org/10.5194/egusphere-2026-2809
Preprint. Discussion started: 6 July 2026

Walker, T. W. N., Kaiser, C., Strasser, F., Herbold, C. W., Leblans, N. I. W., Woebken, D., Janssens, I. A., Sigurdsson, B. D., and Richter, A.: Microbial temperature sensitivity and biomass change explain soil carbon loss with warming, Nat. Clim. Change, 8, 885–889, https://doi.org/10.1038/s41558-018-0259-x, 2018.

Wang, D. T., Welander, P. V., and Ono, S.: Fractionation of the methane isotopologues 13CH4, 12CH3D, and 13CH3D during aerobic oxidation of methane by Methylococcus capsulatus (Bath), Geochim. Cosmochim. Acta, 192, 186–202, https://doi.org/10.1016/j.gca.2016.07.031, 2016.

Whiticar, M. J.: Carbon and hydrogen isotope systematics of bacterial formation and oxidation of methane, Chem. Geol., 161, 291–314, https://doi.org/10.1016/S0009-2541(99)00092-3, 1999.

Whiticar, M. J., Faber, E., and Schoell, M.: Biogenic methane formation in marine and freshwater environments: CO2 reduction vs. acetate fermentation—Isotope evidence, Geochim. Cosmochim. Acta, 50, 693–709, https://doi.org/10.1016/0016-7037(86)90346-7, 1986.

Wickham, H.: ggplot2: Elegant graphics for data analysis, Springer-Verlag New York, 2016.

Wilmoth, J. L., Schaefer, J. K., Schlesinger, D. R., Roth, S. W., Hatcher, P. G., Shoemaker, J. K., and Zhang, X.: The role of oxygen in stimulating methane production in wetlands, Glob. Change Biol., 27, 5831–5847, https://doi.org/10.1111/gcb.15831, 2021.

Xu, H., Huang, L., Chen, J., Zhou, H., Wan, Y., Qu, Q., Wang, M., and Xue, S.: Changes in soil microbial activity and their linkages with soil carbon under global warming, CATENA, 232, 107419, https://doi.org/10.1016/j.catena.2023.107419, 2023.

Yavitt, J. B., Lang, G. E., and Downey, D. M.: Potential methane production and methane oxidation rates in peatland ecosystems of the Appalachian Mountains, United States, Glob. Biogeochem. Cycles, 2, 253–268, https://doi.org/10.1029/GB002i003p00253, 1988.

Yu, X., Song, C., Sun, L., Wang, X., Shi, F., Cui, Q., and Tan, W.: Growing season methane emissions from a permafrost peatland of northeast China: Observations using open-path eddy covariance method, Atmos. Environ., 153, 135–149, https://doi.org/10.1016/j.atmosenv.2017.01.026, 2017.

Zalman, C. A., Meade, N., Chanton, J., Kostka, J. E., Bridgham, S. D., and Keller, J. K.: Methylotrophic methanogenesis in *Sphagnum*-dominated peatland soils, Soil Biol. Biochem., 118, 156–160, https://doi.org/10.1016/j.soilbio.2017.11.025, 2018.